DEVELOPMENT OF TECHNIQUES AND INSTRUMENTATION FOR THE NONDESTRUCTIVE EVALUATION OF MULTI-LAYER INSULATION

NOVEMBER 1972

Battelle
Pacific Northwest Laboratories
Richland, Washington 99352

FINAL REPORT

DEVELOPMENT OF TECHNIQUES AND INSTRUMENTATION FOR THE NONDESTRUCTIVE EVALUATION OF MULTI-LAYER INSULATION

(NASA CONTRACT NAS8-27479)

J. B. Vetrano, Project Director

Prepared for

George C. Marshall Space Flight Center, NASA
Marshall Space Flight Center, Alabama 35812

November 1972

BATTELLE
PACIFIC NORTHWEST LABORATORIES
RICHLAND, WASHINGTON 99352

FOREWORD

This is the final report on a study of nondestructive techniques for the evaluation of multi-layer higher performance thermal insulation. This study was conducted by Battelle-Northwest (Battelle Memorial Institute/ Pacific Northwest Laboratories) for the National Aeronautics and Space Administration, under Contract No. NAS8-27479. Mr. W. N. Clotfelter is the principal contracting officer.

The project director of this program is J. B. Vetrano with technical contributions by H. L. Libby and D. R. Newman.

CONTENTS

LIST OF FIGURES

LIST OF FIGURES (contd)

DEVELOPMENT OF TECHNIQUES AND INSTRUMENTATION FOR THE NONDESTRUCTIVE EVALUATION OF MULTI-LAYER INSULATION

(NASA CONTRACT NAS8-27479)

to

GEORGE C. MARSHALL SPACE FLIGHT CENTER
NATIONAL AERONAUTICS AND SPACE ADMINISTRATION
MARSHALL SPACE FLIGHT CENTER, ALABAMA 35812

INTRODUCTION

The evolvement in the space program of the concept of the reusable integrated launch and recovery vehicle (ILRV) has required further studies of high performance insulation (HPI).[1] Two design constraints resulting from the ILRV concept, the reusability requirement and the effect of environmental cycling resulting from reuse, have led directly to the need of developing nondestructive techniques for the evaluation of HPI.

The main objective of the present project is to develop techniques and instrumentation suitable for the nondestructive evaluation of purged multilayer insulation prior to and after a shuttle orbiter flight. These techniques are desirable because of the possibility that corrosion, compression, or tearing of the insulation will degrade the performance of the insulation during subsequent flights. A second objective is the application of the developed technology to the evaluation of other insulation types.

Three nondestructive evaluation techniques, electromagnetic, thermal and acoustic, have been selected for evaluation in Phase I of this program. The evaluation of each technique follows the order given below, subject to some variations caused by the differences existing in the principles and performance of each technique.

1. Determine optimum operating parameters such as frequencies or temperature differences as a function of defect type and blanket thickness.
2. Determine feasibility of distinguishing total thickness variations from torn or corroded layers.
3. Explore problems and solutions for testing HPI blankets on full-size tanks.
4. Determine essential characteristics for a prototype instrumentation system.

Nondestructive test methods and procedures to be applied to the evaluation of high performance multi-layer insulation have potential for defect detection in other types of insulation and composite structural materials. Since several composites are being considered for use in the shuttle vehicle and funds are limited, no final selections were made by NASA at the start of this program. However in Phase II of the program, the nondestructive evaluation of a second material, goldized kapton provided by NASA, was studied.

Dimensions are given in metric units, but measurements and calculations have been made in the British system of units, given in parentheses.

SUMMARY

The main effort on this program has been expended on evaluating the electromagnetic method, as measurements made using acoustic and thermal techniques showed less promise. The general approach in the electromagnetic method is to simulate the HPI blanket using stacks of double-metallized reflector sheets with paper separators. These stacks, some comprising ten reflector sheets and some comprising fifty reflector sheets, are used as test specimens inspected with eddy current nondestructive test equipment. The eddy current equipment was operated in single-frequency and two-frequency multiparameter modes, and signals obtained were displayed on a cathode ray oscilloscope X-Y presentation.

In general, it was found that simulated compression of the simulated blanket could be detected, the effect of tears or slits in the reflector could be measured, and the resulting signals have different phase angles as a function of frequency and depth of the slitted reflector within the stack. The double-aluminized mylar and the double-goldized kapton supplied by NASA show variations of ±13% and ±19%, respectively, in the thickness-conductivity product from region to region on the sheets. This effect constitutes a rather complicated variable to be discriminated against as signals caused by it also vary in amplitude and phase angle as a function of the distribution of these anomalies with depth in the blanket.

Measurements made with the multiparameter eddy current system in its three- and four-parameter modes demonstrated the ability of the system to discriminate against two variables and three variables, respectively. Using the two-frequency four-parameter mode, independent detection of blanket compression and the presence of a slit pad in a stack of ten pads of reflector sheets was accomplished. At the same time, the effect of inspection coil lift-off and the variation of some reflector sheet conditions were discriminated against successfully. The detection of a one-third compression of the whole simulated blanket, a one-third compression of the top half of the blanket, and a one-third compression of the bottom half of the blanket were also accomplished.

It was observed that the scanning of the inspection coil across the slit position caused some decrease in reliability of the detection of a slit located midway within the stack. This was attributed to the variation of reflector sheet properties and to some edge effect caused by the limited size of the simulated blanket samples. The independent detection of a compressed blanket condition and the presence of a slitted pad at any one of ten pad levels in a ten pad simulated blanket was demonstrated.

The slits, representing torn reflectors, and areas of reflectors from which areas were physically removed, representing corroded regions could not be separately identified by the electromagnetic measurements.

Adjustment of the transformation unit of the two-frequency multiparameter eddy current system is time consuming and requires special skill. Moreover, an increase in the number of operating frequencies will be needed to discriminate against added variables. For example, it is found that the presence of the tank wall and the variation of spacing between it and the blankets represent a new variable. In addition, the use of a limited number of simulated blankets used in this program may bias the results toward greater uniformity. Variations in the HPI material electrical characteristics (thickness - conductivity product) are expected to contribute to variability in results in practical installations.

Considering these factors and the fact that complexity of calibration increases rapidly with an increase in the number of operating frequencies, it is suggested that either an off-line general purpose digital computer or an on-line digital minicomputer be used to process data and perform the calibration and readout functions. A total of five operating frequencies is suggested.

The scanning of the HPI of a full scale tank presents many practical problems. Three alternate ways of performing this function are considered. The first two, removal of the tank from the vehicle and rotating it past automatically positioned coils, and scanning of HPI within the vehicle by coils held on automatically positioned arms, appear to be impractical. The

third method, involving the permanent attachment of inspection coils at selected locations on or within the surface of the outer blanket and the sequential switching of these coils to connect them with the measuring instrument, appears more practical.

In Phase II of the program, it is shown that the same general results reported for the double-aluminized mylar blankets using the multiparameter method were also obtained in the inspection of a simulated blanket made of double-goldized kapton reflector sheets.

It was found that the presence of water between the reflector sheets does not directly affect the measurements at the operating frequencies used. An indirect effect could be observed if the water caused a swelling or settling of the separators in a practical situation.

Acoustical measurements were made by placing the simulated HPI assemblies between a sound source (loud speaker) and a sound sensor (microphone). The results of these measurements showed little promise and further effort in this direction was discontinued.

Thermal measurements were made by placing good and torn or corroded layers of double-aluminized mylar (DAM) in sequence over a heated tank and then scanning the emitted radiation from the front sheet using an infrared scanner. The results indicated that the through transmission steady-state approach is not applicable for the inspection of multilayer insulation as long as two or more intact layers cover the rest, even if inner layers are completely corroded.

STATEMENT OF THE PROBLEM AND APPROACH

The main objective of this program is to develop techniques and instrumentation suitable for the nondestructive evaluation of purged, multi-layer, high performance, thermal insulation before and after a shuttle orbiter flight. Final selection of the HPI materials and configuration has not yet been made by NASA. The following description of the HPI and its relationship to the vehicle is given as being generally applicable for the purposes of the present program; but it is understood that final materials, dimensions,

and arrangements may vary from those described. The effects of different operating conditions and new variables must then be accounted for by extrapolation or by additional measurements.

The HPI is composed of a stack of reflectors and nonmetallic separators and is protected on both inner and outer surfaces with a netting face sheet.[1] A reflector consists of a sheet of double-metallized nonmetallic substrate. Two reflector metals being considered by NASA are aluminum and gold. Two nonmetallic substrates are mylar and kapton. The thickness of the metal layers may be of the order of 300 Å, and the substrate thickness may be approximately 6.35×10^{-9} mm (0.00025 in.). A stack of approximately 20 to 50 reflector sheets and separators comprise a blanket, and at least two blankets and as many as seven may be used to insulate the vehicle tank. A blanket may be approximately 1.27 cm (0.5 in.) thick.

Figure 1 shows a possible arrangement of the HPI in relation to the tank wall which it insulates and the vehicle structure. More than one blanket may be used. Important variables are:

- The presence of torn or corroded reflectors,
- Compression of the blankets,
- The variation in spacing between the blankets and the tank wall,
- Crumpling of the blankets,
- Distance of purge bag from blanket in reference to available space for inspection sensors,
- Distance from blankets, or tank to vehicle structure, and
- The presence of other structural components, metal or nonmetal.

It is desired to distinguish total thickness variations from torn or corroded composite layers, to study practical problems related to the inspection of insulation on full scale tanks, to define mechanical fixtures required for scanning large tanks, and to determine characteristics considered essential for a prototype instrumental system.

Actual HPI blanket specimens were not available for use in this program, but some HPI sheets of double-aluminized mylar (DAM) and double-goldized kapton (DGK) were furnished by NASA. In addition, some locally

procured DAM and some DAM procured from a vendor recommended by a NASA representative were used. Simulated blankets were made up from sheets of DAM and DGK, using sheets of paper for separators in most of the electromagnetic measurements.

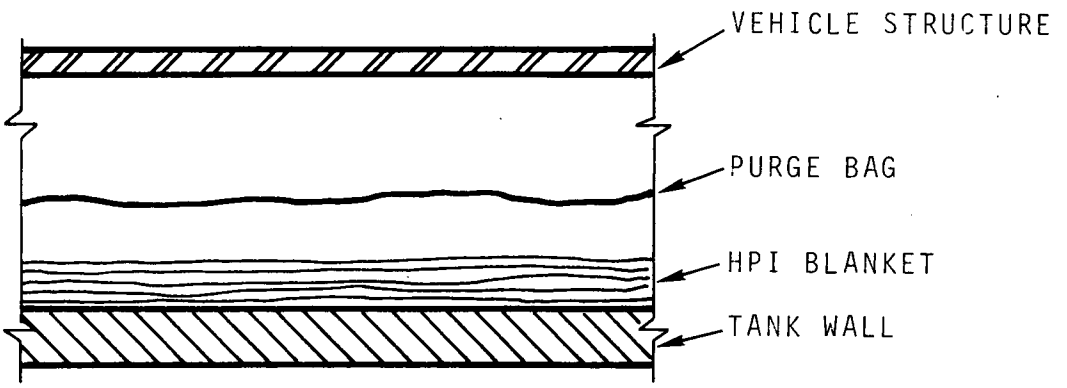

FIGURE 1. High Performance Insulation (HPI) Blanket Position with Respect to Tank and Vehicle Structure

Electromagnetic measurements were made using single-frequency and two-frequency multiparameter[2,3] techniques. The relative changes of the impedance of one or more induction coils placed adjacent to the simulated blankets were used as a means to detect the presence of the blanket and defects within the blanket. Acoustic measurements were made using low frequency techniques. Thermal investigations were made by heating a tank and noting temperature gradients on the surface of a HPI blanket mounted on the tank.

PHASE I. DEVELOPMENT OF TECHNOLOGY FOR EVALUATING MULTI-LAYER INSULATION

Three nondestructive techniques, electromagnetic, acoustical and thermal were evaluated in this phase of the program.

MULTIPARAMETER ELECTROMAGNETIC INSPECTION SYSTEM

A photograph of a two-frequency multiparameter electromagnetic or eddy current inspection system used in making some of the measurements in this program is shown in Figure 2. The system consists of an inspection probe A-1 and a reference probe A-2 shown in place on simulated high performance thermal insulation blankets B-1, B-2 and B-3 at the right side of the photograph. A two-frequency eddy current inspection device C[(4)] operating simultaneously at 100 and 300 kHz is shown at the left side of the photograph, and a transformation unit D consisting of six dual sine-cosine potentiometers and associated amplifiers is located near the center of the photograph. The four knobs above the transformation unit operate vernier controls connected in four of the sine-cosine potentiometer circuits within the transformation unit. A storage type cathode ray oscilloscope, which is used to monitor the system signals, is not shown in Figure 2. The six dual sine-cosine potentiometers and associated circuits serve as signal pattern rotators and play an important role in the multiparameter operation.

Inspection coils A-1 and A-2 are identical; each has a single winding 5.08 cm (2.0 in.) diameter wound with 20 turns of No. 31 AWG magnet wire. The operation of this equipment is flexible. It can be used as a single-frequency eddy current device operating at either 100 kHz or 300 kHz, or as two single-frequency devices operating simultaneously but using the same inspection coil assembly, or finally as a two-frequency multiparameter device.

B

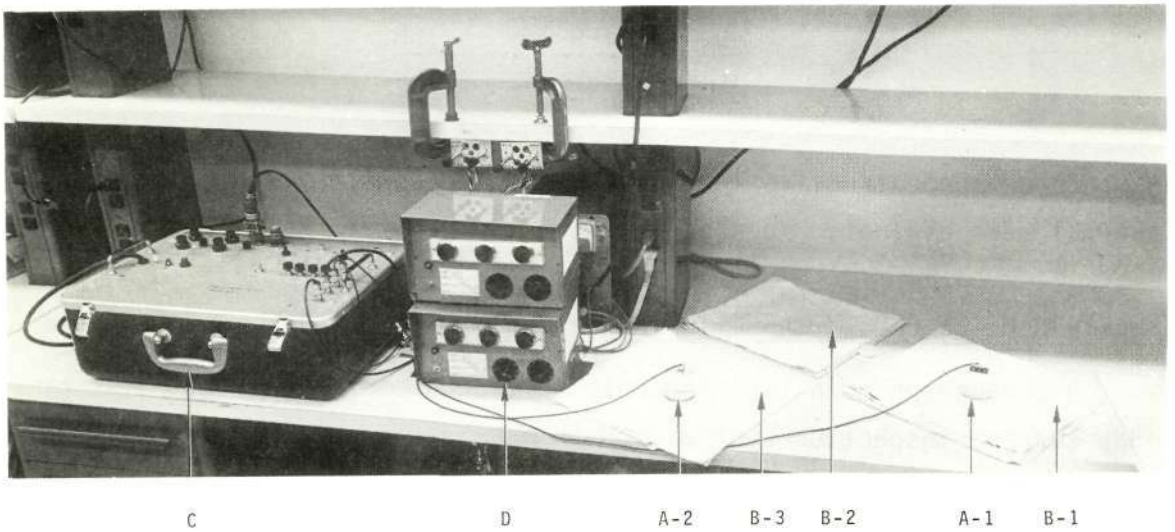

FIGURE 2. Two-Frequency Multiparameter Eddy Current Inspection System with Inspection Coils and Simulated High Performance Insulation Blankets

SIMULATED THERMAL INSULATION BLANKETS

Three different simulated blankets are shown in Figure 2. These blankets consist of double-aluminized mylar (DAM) sheets with paper separators. They are assembled or stacked so that some separators may be removed to simulate a compressed separator condition. Also, normal sheets may be replaced by ones having slits to simulate torn sheets. Blanket B-1, associated with inspection probe A-1 in Figure 2, serves as a nominal "not compressed" specimen or as one with torn or slit sheets as desired. This nominal specimen also serves for determining the effect of inspection probe-to-blanket spacing (lift-off) effect. Blanket B-2, the blanket not associated with either probe in Figure 2, serves to simulate a compressed separator condition. This condition is obtained by using fewer separators than are used in the nominal blanket. Blanket B-3, associated with the reference probe A-2 in Figure 2, serves as a reference blanket. It is also made up by stacking DAM sheets and paper separators.

Three different types of DAM material are used in this program and are designated DAM-1, DAM-2 and DAM-3. DAM-1 material was furnished by NASA and consists of circular sheets about 30 cm (12 in.) diameter. DAM-2 is material obtained locally and has an electromagnetic effect about 20% of that produced by the NASA material. DAM-3 is material recently procured from a source recommended by NASA and is similar to the DAM-2 material. One type of double-goldized kapton designated as DKG-1 furnished by NASA for use in Phase II of the program is also used, and is discussed elsewhere in this report.

Blankets B-1 and B-2 are made up using the locally-produced DAM material, and blanket B-3 is made up using the material supplied by NASA.

The "nominal" blanket B-1 and the "compressed" blanket B-2 are made by stacking ten pads of locally procured DAM material. Each pad is made by placing five DAM sheets approximately 30.48 x 30.48 cm (12 x 12 in.) within a fold of paper as shown in Figure 3. The sheets of DAM material are placed within the paper fold without separators between them and the assembly is stapled as shown. Blanket B-1 is made by stacking ten of the pads with one paper spacer between each pad as shown in Figure 4. The thickness of the completed blanket is exaggerated in the drawing since it is only about 0.32 cm (0.125 in.). Blanket B-2 is similar to blanket B-1 except that the single paper sheet between the pads is omitted to simulate a compressed separator condition. Blanket B-1 will sometimes be referred to as a 3-separator blanket, and blanket B-2 will be referred to as a 2-separator blanket.

Blanket B-3, the reference blanket, is made by stacking ten sheets of the NASA DAM material with a layer of paper 0.102 mm (0.004 in.) thick between each DAM sheet, and one layer of paper at the top and bottom of the stack.

Two slit pads, each having slits cut in each of the five DAM sheets, are assembled in Figure 5.

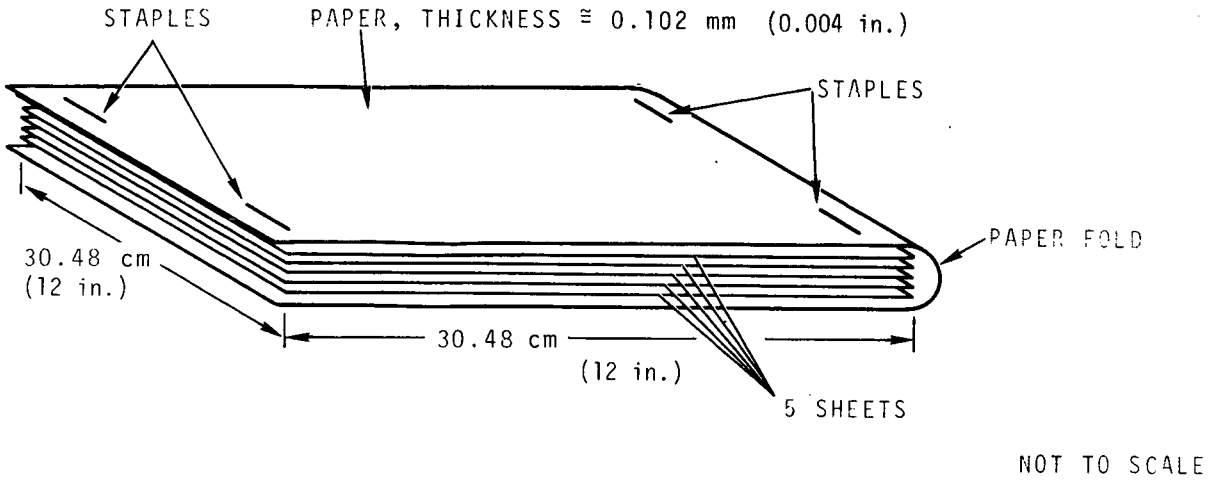

FIGURE 3. Composition of One Five-Sheet Double-Aluminized Mylar (DAM) Pad

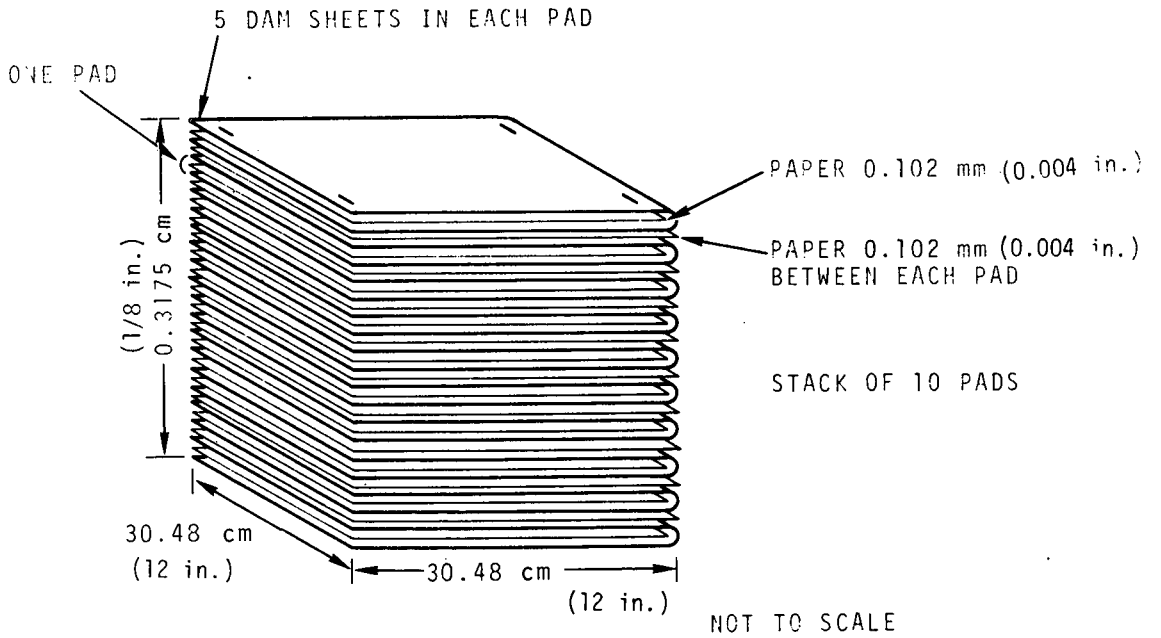

FIGURE 4. Composition of Simulated Blanket

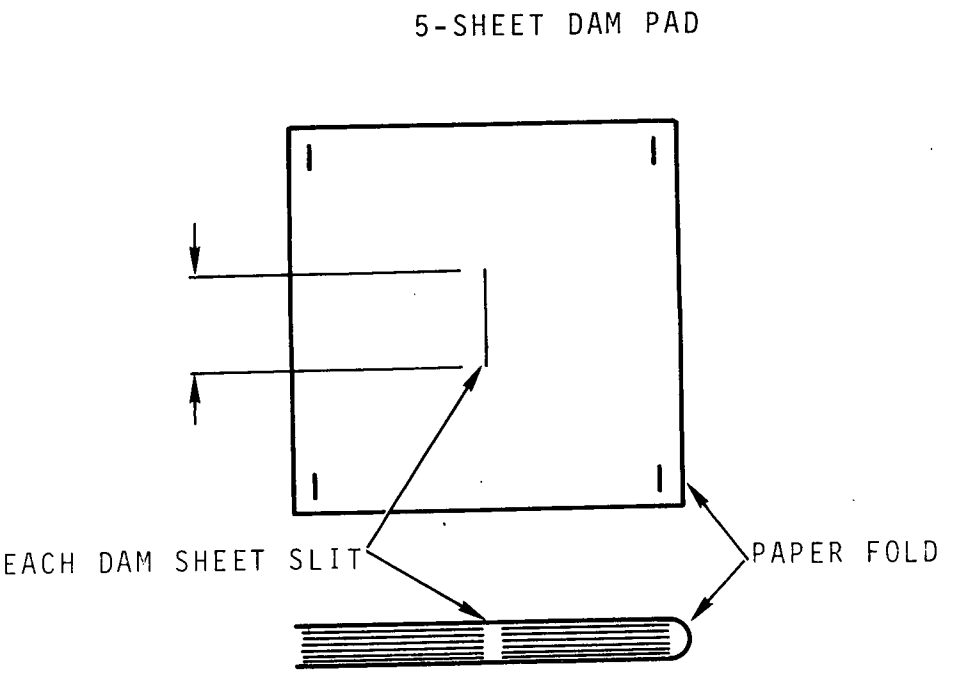

SLIT PAD	LENGTH OF SLIT
SP-a	5.08 cm (2.0 in.)
SP-b	7.6 cm (3.0 in.)

NOT TO SCALE

FIGURE 5. Composition of Slit Pad

The variation of inspection probe-to-blanket spacing (probe lift-off) is produced by use of one or more paper separators 0.102 mm (0.004 in.) thick or by use of a cardboard spacer 0.4064 mm (0.016 in.) thick. Other combinations of one or more reflector sheets are possible and are also used.

EXPERIMENTAL PROCEDURE AND PRINCIPLES OF OPERATION

The procedure can best be explained by referring to Figure 6 which is a block diagram of the equipment pictured in Figure 2. First, use of this equipment as a single-frequency device to make comparative measurements of the DAM and DGK composites will be described. Next, a typical procedure

will be described in which the device is used in its two-frequency mode to detect two parameters or variables and to discriminate against the signal effects two other parameters. The two parameters to be detected are the presence of a slit pad at pad level 5 in blanket B-1, p_3, and the presence of separator compression, p_4, as represented by blanket B-2. The two parameters to be discriminated against are the inspection probe lift-off p_1 at blanket B-1 (3 separator condition) and the effect of the presence of varying blanket electrical conditions p_2. The latter effect is observed when the inspection probe is moved from place to place within a 10 cm (4 in.) square at the top center of the pad.

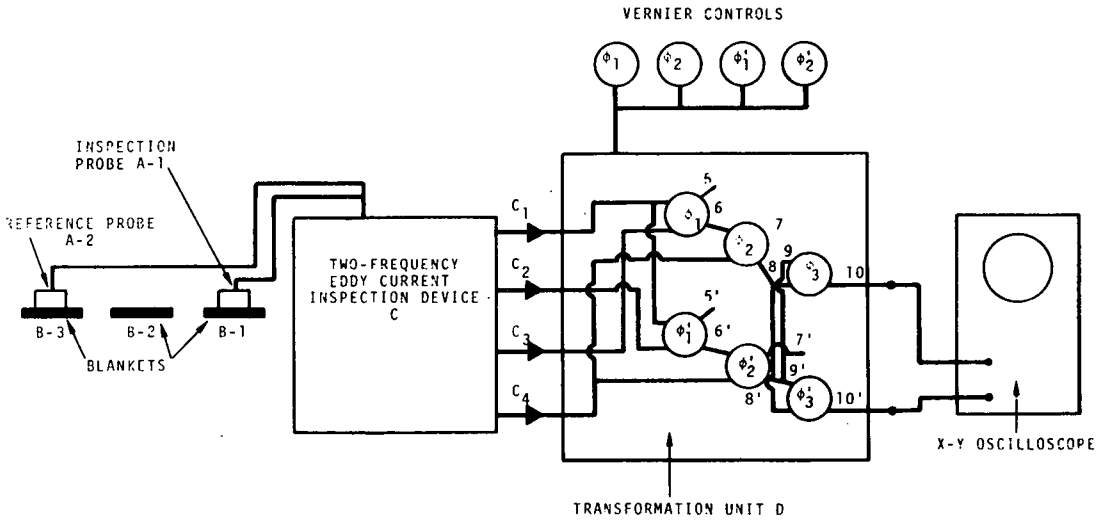

FIGURE 6. Block Diagram of Multiparameter Eddy Current Inspection System

Initial instrument adjustments are similar for both single-frequency and two-frequency operation. Differences occur in the selection of output circuits and in the increased complexity of calibration adjustments in the case of multiparameter two-frequency operation. In any event the inspection probe A-1 is first placed on blanket B-1, Figure 2, or other specimen, and centered. Next, the reference inspection probe A-2 is similarly placed on the reference blanket B-3, or other reference specimen. The ac bridge

controls of the eddy current device are then adjusted to produce an ac null signal on both 100 and 300 kHz channels at the respective amplifier output test points. Next the dc balance controls are adjusted to near null output at the phase detector output terminals C_1, C_2, C_3, and C_4. Amplifier gain controls are set to give output signals within the dynamic range of the instrument system.

Single-frequency operation at 100 kHz is obtained by viewing the signals at terminals 5 and 6 (Figure 6) using an X-Y oscilloscope. Single-frequency operation at 300 kHz is obtained by similarly viewing the signal outputs at terminals 5' and 6'. The signal patterns thus viewed can be oriented on the oscilloscope screen by turning the shaft of the corresponding signal pattern rotator ϕ_1 or ϕ_2.

The patterns thus displayed show changes in the ac impedance of the inspection coils as affected by different probe-inspection specimen conditions. The oscilloscope presents a single beam spot for fixed specimen conditions, and produces a pattern as the specimen conditions change. The spot represents the phasor output of the inspection coil bridge in the instrument.

Multiparameter operation is obtained by connecting the X-Y oscilloscope to output terminals 10 and 10' in Figure 6, and by adjusting signal pattern rotator controls ϕ_1, ϕ_2, ϕ_3, ϕ_1', ϕ_2' and ϕ_3' to obtain the desired discrimination and separation of signals.

The use of a storage type X-Y oscilloscope in all cases is found to be very convenient for storing the signal patterns.

SINGLE-FREQUENCY MEASUREMENTS

Relative inspection coil impedances were measured at 100 kHz for the following single sheet HPI composites:

Specimen Code	Description
DAM-1	Double-aluminized mylar furnished by NASA
DAM-2	Double-aluminized mylar obtained locally
DAM-3	Double-aluminized mylar from vendor recommended by NASA
DGK-1	Double-goldized kapton, furnished by NASA

The results are shown in Figure 7. The reactance axis was established by bringing a piece of ferrite up to the empty (unloaded) coil, and the orientation of this axis was adjusted vertically by turning the shaft of signal pattern rotator ϕ_1, Figure 6. The composites DAM-2 and DAM-3 appear to be nearly equivalent electrically as do DAM-1 and DGK. However, the latter two have a thickness electrical conductivity product between four or five times that of the DAM-2 and DAM-3.

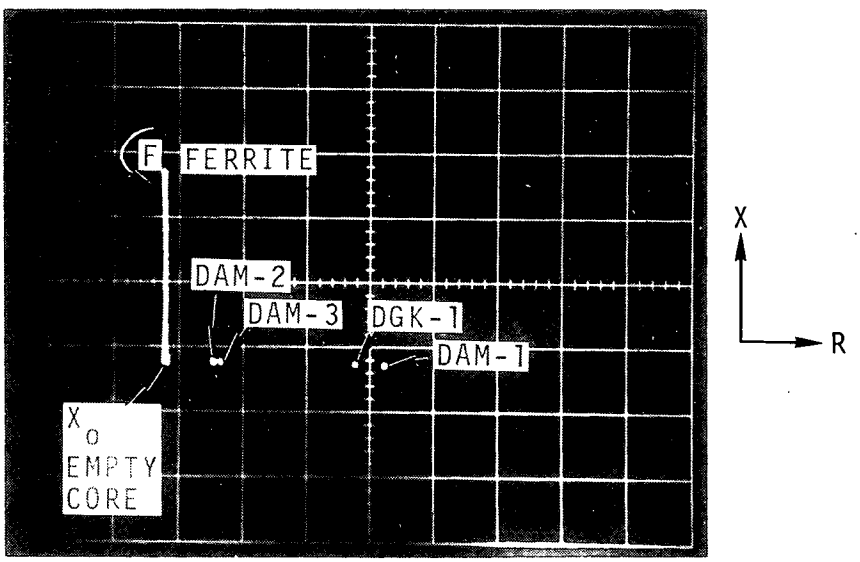

FIGURE 7. Inspection Coil Relative Impedance for Single Reflector Sheets

During many of the measurements it is noted that the instrument output varies as the inspection coil is moved from point to point on the simulated blankets. This variation has been traced to changes in the reflector sheets

from point to point. This is illustrated in Figures 8a, b, c and d which shows phasor signals obtained at four different locations on single sheets of DAM-1, DAM-2, DAM-3, and DGK-1 respectively. These variations are severe, representing ±13% changes in the DAM-1 material, ±17% changes in DAM-2 material, ±9% in DAM-3 material and ±19% changes in DGK-1 material. The instrument sensitivity is different for each of the four Figures 8a, b, c and d and is not shown. These figures show only relative readings obtained at different places on the same material.

Signal loci displays for several different inspection conditions using pads made up of DAM-2 composite material are shown in Figures 9 and 10. The complex plane signal loci obtained by varying the number of pads from one to ten is shown in Figure 9 for 0.3048 mm (0.012 in.) and 0.203 mm (0.008 in.) thick separators between each pad. The operating frequency is 100 kHz and the diameter of the inspection coil is 5.08 cm (2 in.).

The effects of the presence of a 5.08 cm (2 in.) long tear (or slit), first in the top pad (Pad No. 1) and secondly in pad No. 5, halfway down the stack of ten pads are shown in Figure 11. All five DAM sheets in the pad simulating the tear were slit.

The two loci shown in Figure 10 have been displaced with respect to each other by 6 mm (1/4 in.) for ease in noting differences. The operating frequency is 300 kHz and the same 5.08 cm (2 in.) diameter inspection coil is used. The signal obtained by traversing the inspection coil over the region of the tear (or slit) when the tear is in the middle pad (Pad No. 5) has a greater lagging phase angle than when the tear is in the top pad. This change in signal phase angle is expected, being the result of the increasing lagging phase angle of the eddy currents as depth increases.

The data shown in Figures 9 and 10 were obtained at low instrument sensitivity. At higher sensitivities undesirable signal variations were noted when traversing the inspection coil. These may be caused by electrical conductivity or metal thickness variations in the DAM sheets being used.

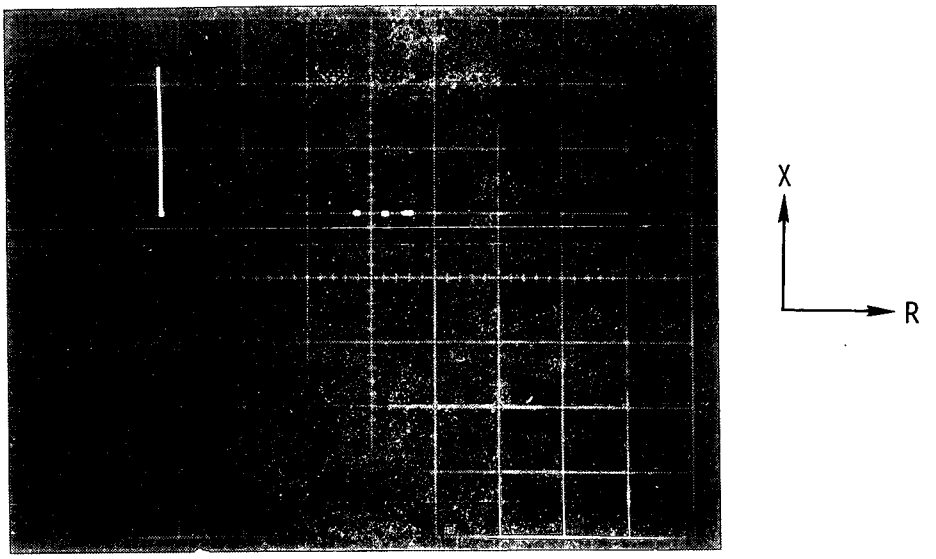

a - DAM-1

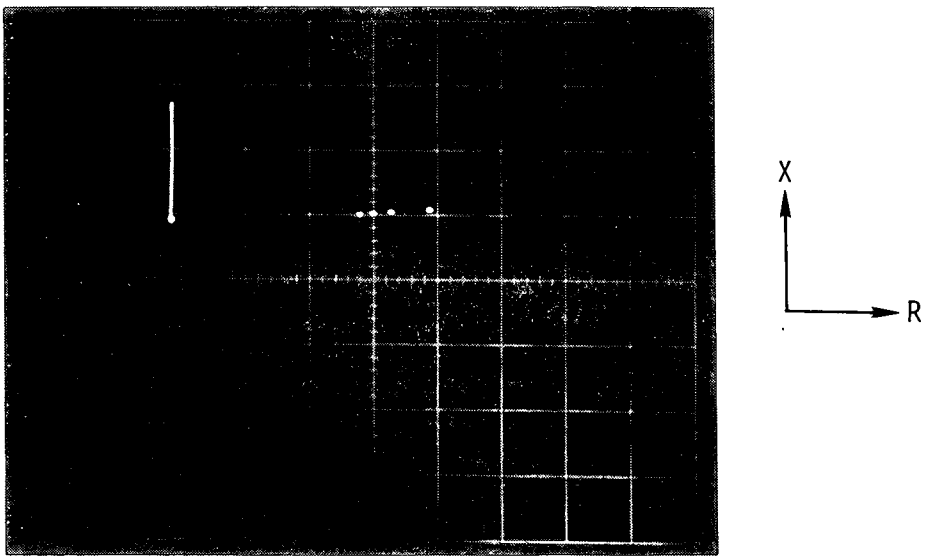

b - DAM-2

FIGURE 8. Nonuniformity of DAM and DGK Material

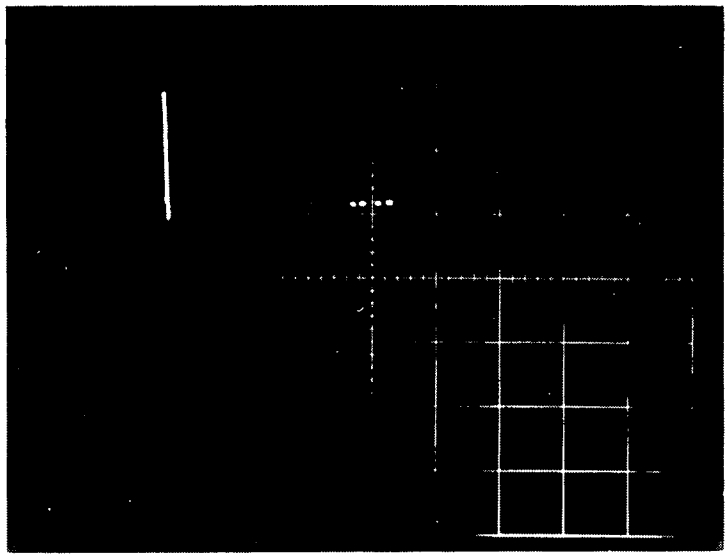

c - DAM-3

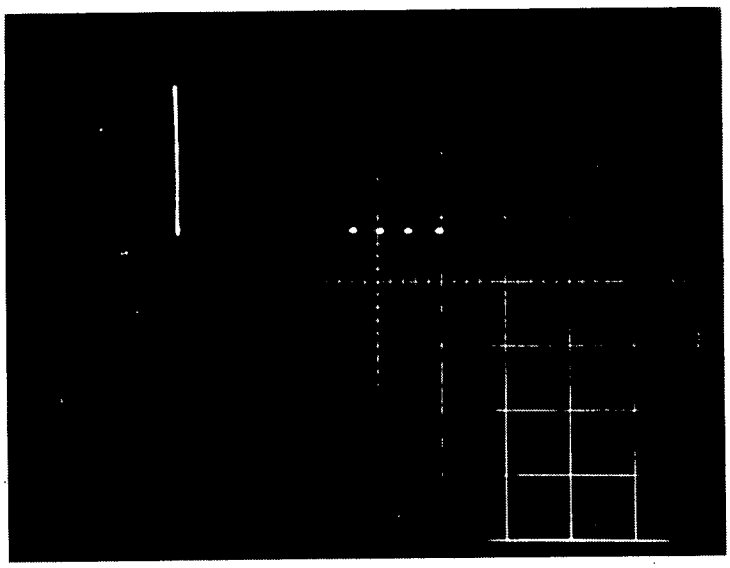

d - DGK-1

FIGURE 8. (contd)

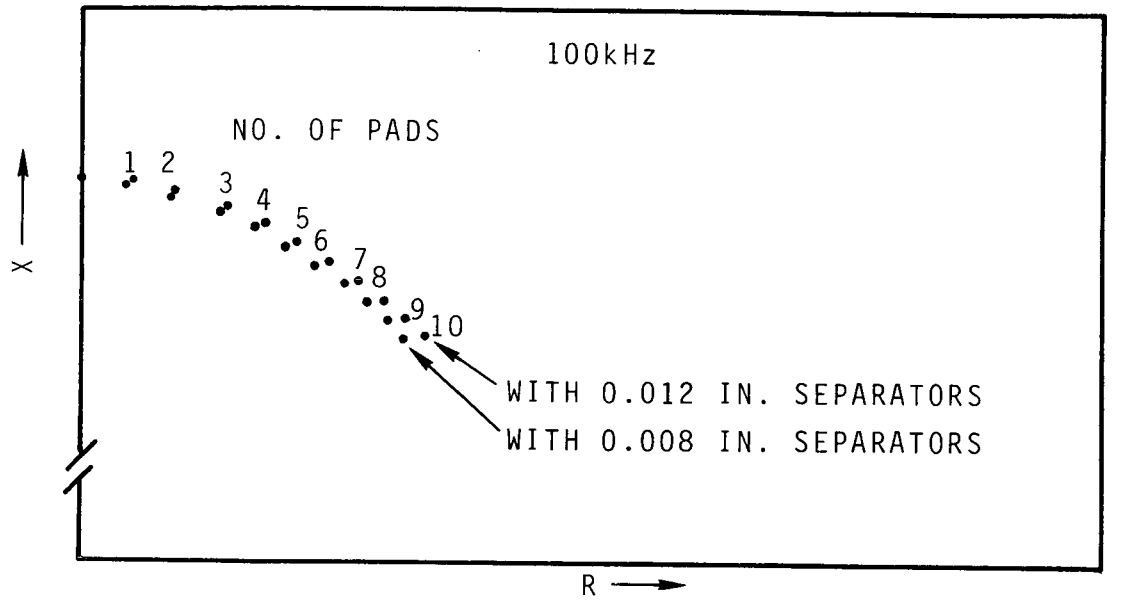

FIGURE 9. Effects of Changing Amount of Insulating Material and Separator Thickness on Eddy Current Signals

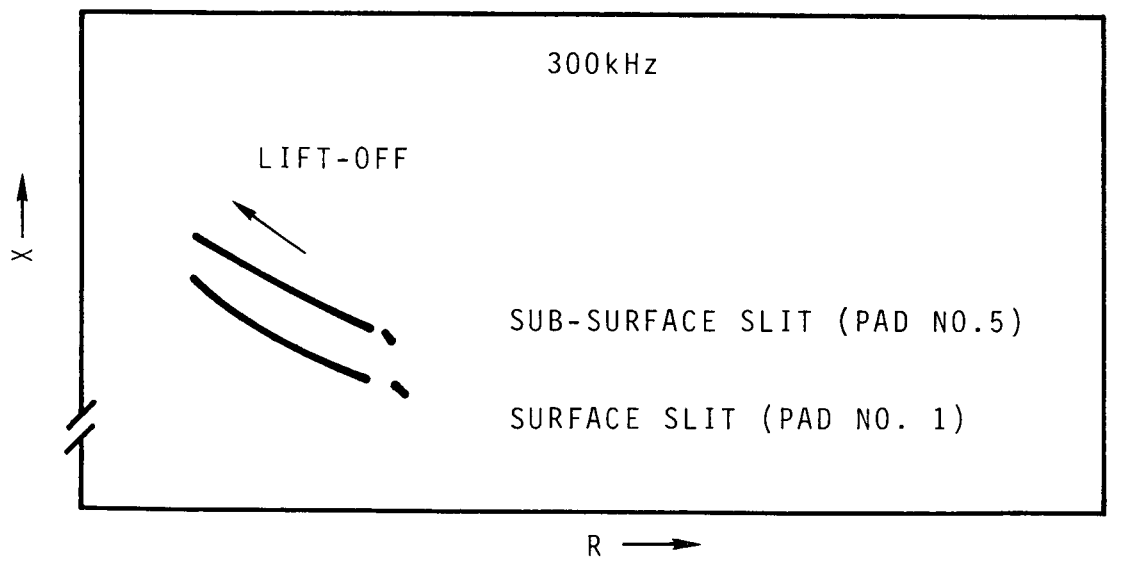

FIGURE 10. Effects of Surface and Subsurface Slits (or Tears) on Eddy Current Signals

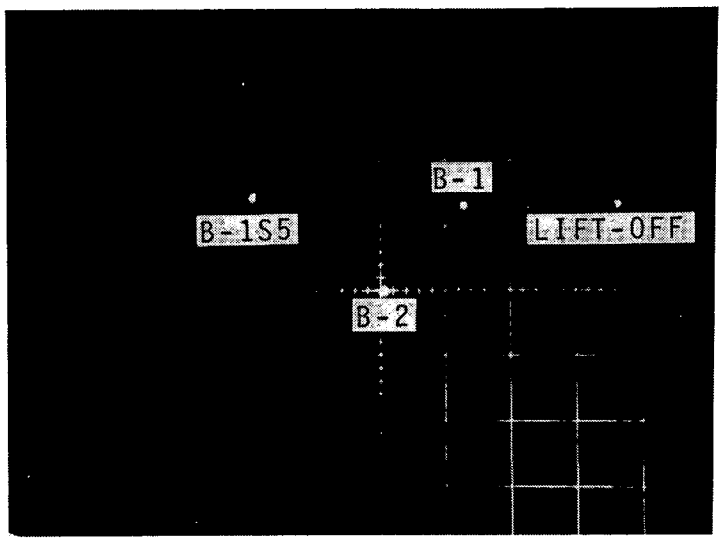

FIGURE 11. Detection of Compressed Blanket (B-2) and Discrimination Against Lift-Off and Against a Slit in a Pad at Level 5 (B-1-S5)

TWO-FREQUENCY OPERATION

The single-frequency eddy current inspection system has the capability of discrimination between two signals, whereas the two-frequency system can discriminate between four signals. The two-frequency system is evaluated because of the number of variables present in the assembled blankets and final installation. Additional details of the theory of the multiparameter eddy current test method are given in the section titled "Single-Frequency Multiparameter Measurements."

PARAMETER DISCRIMINATION ADJUSTMENT

The inspection probe A-1 is alternately exposed to the conditions of varying lift-off distance and varying position of the probe within a 10-cm (4 in.) square at the center of blanket B-1. The signal outputs at terminals 7 and 8 of the transformation unit are displayed on the X-Y oscilloscope, with terminal 7 connected to the horizontal channel and terminal 8 connected to the vertical channel. In general, the signals

produced by the nominal blanket condition, lift-off, and the varying position of the probe within the 10-cm (4 in.) square surface region will give three dots on the storage oscilloscope screen which do not appear in line. Each dot represents the tip of the phasor signal for a particular inspection coil-reference coil, bridge balance output signal.

In order for these signals to be discriminated, they must be in line. It is noted that these signals appear singly because the inspection coil can be presented to only one set of specimen conditions at a time. The storage oscilloscope is used to store the signals for comparison purposes. The three aforementioned dots, or phasor signal representations, can be brought in line by adjusting the signal pattern rotator ϕ_1, shown in Figure 6, in a series of iterative adjustments as the inspection coil is presented alternately to the three blanket conditions. After the three signals have been aligned, the alignment can be brought to a horizontal position. In this condition, the two test specimen conditions to be discriminated produce no signal at terminal 8.

This procedure is repeated with the oscilloscope connected to terminals 7' and 8'. The signal pattern rotator ϕ_1' is adjusted to give alignment of the phasor tip points, and rotator ϕ_2' is adjusted to rotate the aligned points to a horizontal position. When these adjustments have been completed, it is noted that the two parameters to be discriminated produce no output signals at terminals 8 and 8'. The other two variables, in general, will produce signals at these two circuit points if their signals are algebraically independent.

One of the two remaining parameters may be discriminated against at terminal 10 by adjustment of ϕ_3. Thus starting with signals from four parameters, two of these signals from parameters p_1 and p_2, have been discriminated against; parameter p_3 is indicated by a signal at terminal 10, and parameter p_4 is indicated by a signal at terminal 10'. It should be emphasized that any other parameter or parameters for which the transformation unit has not been adjusted may give signal indications on all output terminals.

THREE-PARAMETER RESULTS

Figures 11 and 12 show the separation of signals from simulated compression of an insulation blanket (2 separators) and a slit (SP-a) in a pad at level 5 in a ten-pad blanket (B-1-S5) while discriminating against inspection coil lift-off of 0.4064 mm (0.016 in.). Since two parameters can be discriminated against by using only two of the signal pattern rotators, the results shown were obtained using only the rotators ϕ_1' and ϕ_2'. They were adjusted first so that signal points from blanket B-1 (3 separators), lift-off and the slit at pad level 5 (B-1-S5) appeared nearly in a horizontal line with minimum vertical components, as shown in Figure 11. The compressed blanket (B-2) then produced the signal shown which has appreciable vertical component. Thus, compression is read on this channel, while the signals caused by the lift-off of 0.4064 mm (0.016 in.) and the presence of a slit pad at level 5 in the ten-pad blanket are discriminated against.

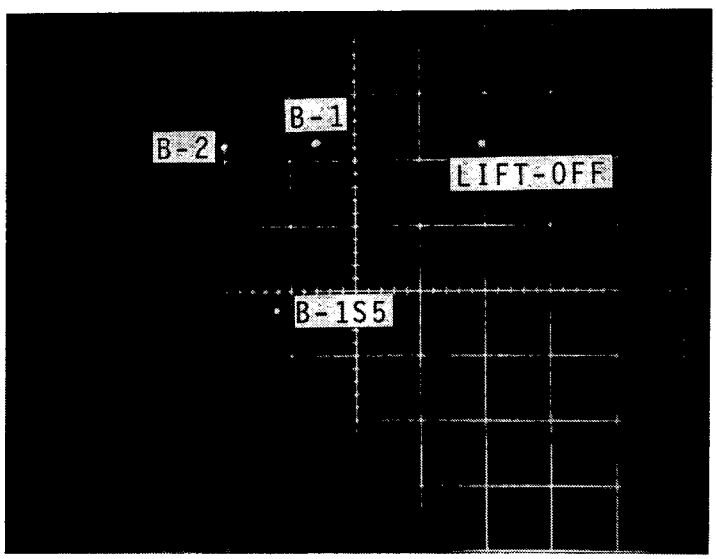

FIGURE 12. Detection of a Slit in a Pad at Level 5 (B-1-S5) and Discrimination Against Compression of Blanket (B-2) and Lift-Off

Next ϕ_1' and ϕ_2' were readjusted to discriminate against lift-off and the compressed blanket condition; and the presence of the slit pad at level 5 is indicated as shown in Figure 12. In this example, the same two rotators were used to obtain the results shown at different times. Two sets of rotators could have been used to provide two output channels operating concurrently, and would be so used in a practical application.

These results are subject to qualification because of some simplification in the taking of the data. The inspection coil was placed directly over the known location of the slit at level 5 when the data was taken. The degradation of signal separation caused by scanning of the inspection coil across the slit region is discussed in the next section.

FOUR-PARAMETER RESULTS

The results obtained with a four-parameter system are shown in Figure 13. The parameters here are inspection coil lift-off, compression of a blanket (B-2), slit in a pad (SP-b) at level 5 (B-1-S5) and variation of electrical characteristics of blanket B-1 over 4 locations in a 10-cm (4 in.) square area in the center of the blanket (B-IV). This illustrates identification of the simulated compression of a blanket and the existence of a slit in a pad at level 5, while at the same time discrimination is effected against inspection coil lift-off and variation in blanket characteristics over a 10-cm (4 in.) square region. The complex plane signal pattern in Figure 13 was obtained by displaying the signals at terminals 9 and 10 in Figure 6 after rotators ϕ_1 and ϕ_2 were adjusted to provide the needed discrimination against the undesirable signals caused by inspection coil lift-off variation and the variation of blanket characteristics. Since the two parameters represented in Figure 13 appear as two vectors (or phasors) they can be separated by manipulation of rotator ϕ_3 and ϕ_3' in Figure 6. This was not done here, but the adjustment of ϕ_3 is almost correct for reading the compressed blanket condition (B-2).

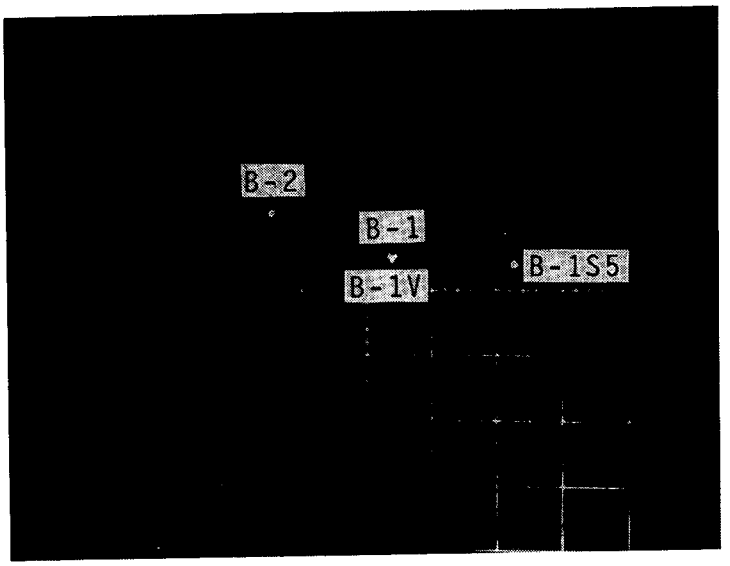

FIGURE 13. Detection of Compressed Blanket (B-2) and Slit in a Pad at Level 5 (B-1-S5) and Discrimination Against Lift-Off and Variation in Electrical Characteristics of Blanket B-1 (B-IV)

The discrimination of the inspection coil lift-off effect at several intermediate lift-off values is shown in Figures 14 and 15. Here, the signals observed at terminals 7 and 8 and terminals 7' and 8' in Figure 6 are shown for several lift-off conditions. The ability to discriminate against lift-off signals caused by lift-off distances of 0.102, 0.204, 0.306 and 0.408 mm (0.004, 0.008, 0.012 and 0.016 in.) is indicated by the array of corresponding phasor points in line in both Figures 14 and 15. Note that a signal pattern as shown in Figure 13 will be obtained by displaying signals at terminal 8 versus those at terminal 8'.

The effect of uneven blanket compression on the separation of signals was investigated next. Results of compression of the bottom half of the blanket are shown in Figure 16, (symbol B-2-32); and results of the compression of the top half of the blanket are shown in Figure 17, (symbol B-2-23). Both of these figures are in contrast to Figure 12. Figures 15 and 16 show that the compression signals are affected only in their amplitude and separability appears to be not adversely affected.

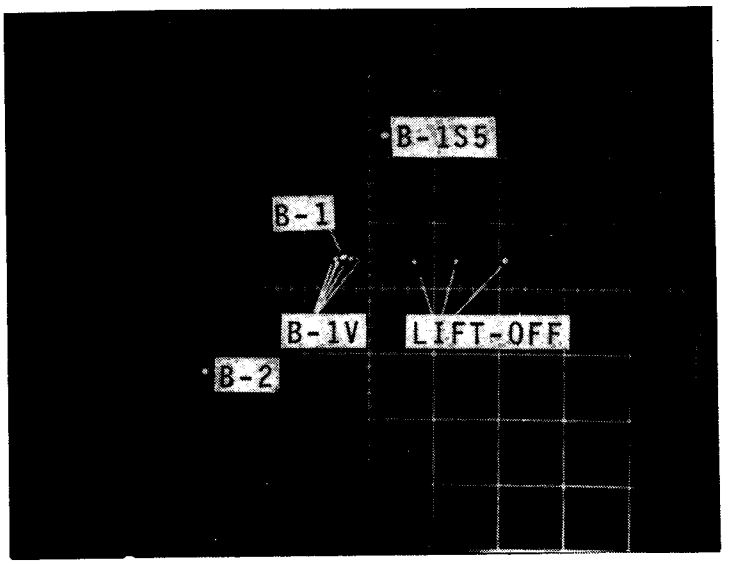

FIGURE 14. Discrimination Against Inspection Coil Lift-Off Effect over a Range of Lift-Off Distance from 0 to 0.408 mm (Terminals 7, 8, Figure 5)

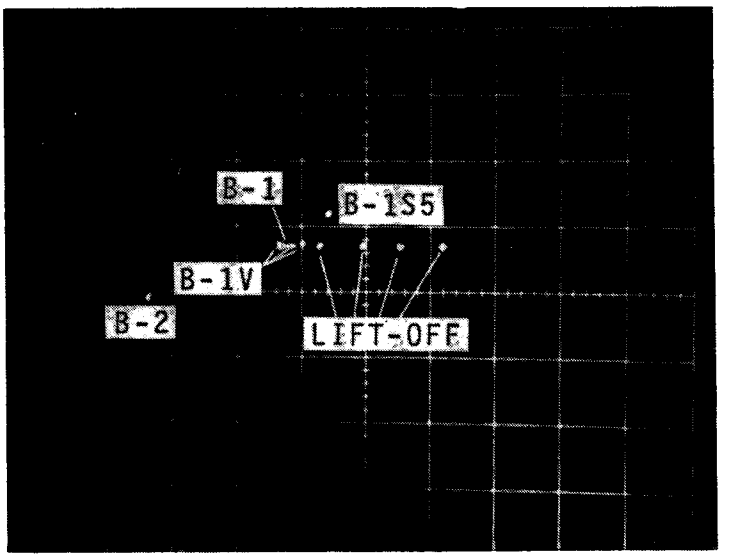

FIGURE 15. Discrimination Against Inspection Coil Lift-Off Effect over a Range of Lift-Off Distance from 0 to 0.408 mm (Terminals 7', 8', Figure 5)

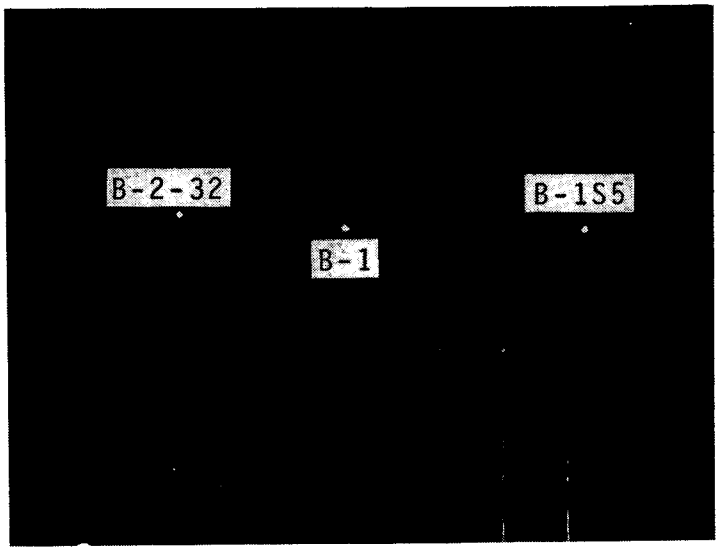

FIGURE 16. Detection of Compression of Bottom Half of Simulated Blanket

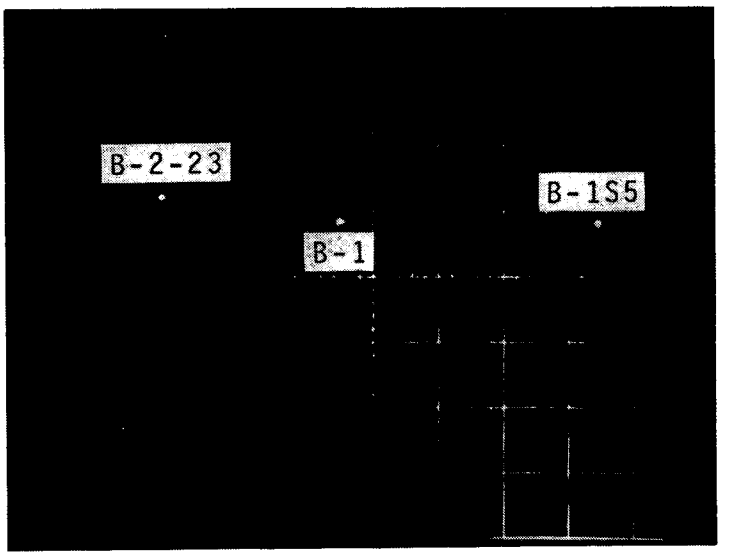

FIGURE 17. Detection of Compression of Top Half of Simulated Blanket

It should be emphasized that the phrase "identification of the simulated compression of a blanket and the existence of a slit in a pad at level 5" should be qualified. The inspection probe in this instance is placed over the known location of the slit in the same position used in the calibration procedure. If the inspection probe is moved across the surface of the blanket over the region containing the slit, the resulting signal is quite complex and would not produce as distinct a separation of signals as indicated by Figure 12. The signals resulting from moving the inspection coil across the slit region at 1.27 cm (0.5 in.) intervals in each of four directions from the center position are shown in Figures 18a to d. The main impact of the differences between patterns shown in Figure 12 and those in Figure 18 is that the source of the signals in Figure 12 can be properly identified even though the conditions causing the two signals are present simultaneously within the field of the inspection probe. The variety of signals resulting from scanning the inspection coil across the slit region, as exemplified by Figure 18, reduces the reliability of identification of the compressed blanket condition and the slit when they occur simultaneously within the field of the coil. The points labeled 6, 7, and 8 may be ignored since it has been determined that their large undesirable excursions are caused by edge effect. This edge effect was found to be appreciable whenever the inspection coil was more than about 5.08 cm (2.0 in.) from the center of the 30 by 30 cm (12 x 12 in.) simulated blanket.

The detection of the slit pad at different levels within the blanket is shown in Figure 19. Independent readout of the compressed blanket and the slit pad at all ten levels is maintained, as well as discrimination against inspection coil lift-off and variation of blanket characteristics (B-IV). These blanket variations may be a source of difficulty in the inspection of actual HPI blankets. They are apparently caused by local variations in conductivity or thickness of the metallized portion of the reflectors.

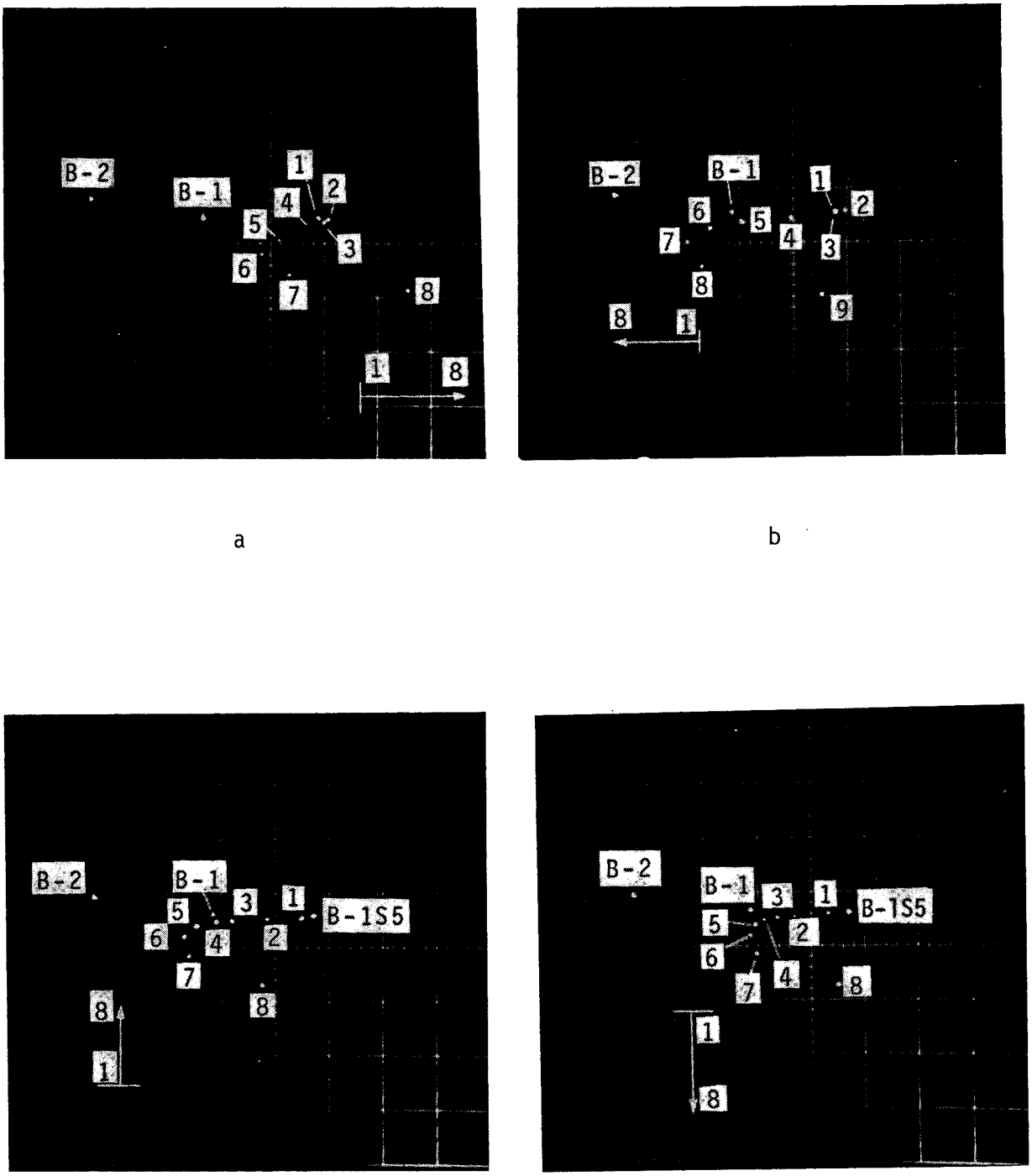

a b

c d

FIGURE 18. The Effect of Moving Inspection Coil with Respect to Slit; Test Coil Moved in 1.27 cm Intervals from Center Position in Direction Shown

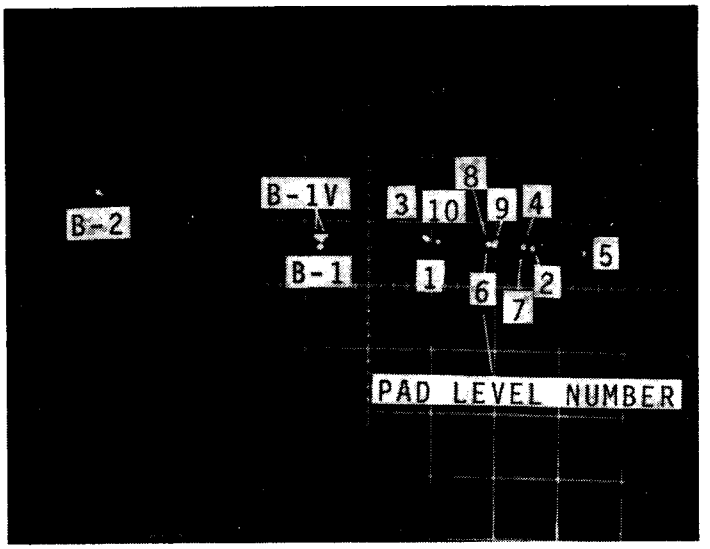

FIGURE 19. Detection of Slit Pad at Ten Different Levels Within a 10-Pad Blanket

COMPLEXITY OF CALIBRATION ADJUSTMENTS

Adjustment of the transformation unit of the multiparameter eddy current system is time consuming and requires special skill. Added operation frequencies will probably be needed in a practical system since the effect of tank proximity has not yet been taken into consideration. In addition, the use of just two specific blankets as the variable blankets in this work may bias the results toward better uniformity. Variations which have been observed in DAM material electrical characteristics are expected to contribute to variability in results.

The complexity of the calibration adjustments increases as the number of separating frequencies is increased. A computer method is under study which has good potential for reducing the complexity of the calibration procedure.

SINGLE-FREQUENCY MULTIPARAMETER MEASUREMENTS

Although a single-frequency eddy current system using a single inspection coil can discriminate between only two parameters, a single frequency, two-channel system using two inspection coils having different diameters can

discriminate between more than two parameters.[5] The inspection system used in implementing these principles consists of two single-frequency eddy current inspection devices operating at 400 kHz and two double inspection coil assemblies. Each inspection coil assembly consists of two excitation-sensing coil parts, one having a diameter of 7.62 cm (3 in.) and the other 3.81 cm (1.5 in). The two coils in each assembly are mounted coaxially and co-planar in a fixed position so that they can be placed parallel and close to the surface of the simulated blanket.

The excitation coils comprise 10 turns of No. 31 AWG(B&S) magnet wire, and the sensing coils comprise 50 turns of No. 36 AWG(B&S) magnet wire. One assembly is used for inspection and the other as a reference with both sets of coils connected in comparator circuits. The excitation coils are driven in series with a single-frequency current. The signals from the two larger sensing coils are fed to one eddy current instrument and the signals from the two smaller sensing coils are fed to the second instrument.

Complex plane eddy current signal loci were obtained with this coil assembly for four simulated insulation blanket conditions. A blanket is made by stacking ten pads of assembled aluminized mylar sheets and paper separators. Each pad consists of five sheets of double-aluminized mylar sheets and paper separators. Each pad consists of five sheets of double-aluminized mylar, DAM-2 (DAM) 30 x 30 cm (12 x 12 in.) obtained locally. Five sheets of the DAM-2 material being used are approximately equivalent electrically to one layer of the DAM-1 material furnished by NASA. Separators are simulated by using paper spacers. In this test, each group of five DAM sheets is separated by three sheets of 0.102 mm (0.004-in.) thick paper. Actually, each pad of five DAM sheets is formed by placing them within a fold of the paper, resulting in a pad of five DAM sheets of local material between two sheets of 0.102 mm (0.004-in.) thick paper as shown in Figure 3. The paper is stapled at the open edges to protect the DAM sheets during handling.

A nominal blanket is made up with a stack of ten of these pads, with an extra 0.102 mm (0.004-in.) thick paper sheet between each one, giving a simulated spacer 0.3048 mm (0.012-in.) thick between each group of five DAM sheets. The crushing of separators is simulated by withdrawing the extra sheets, reducing the separation between groups of five sheets from 0.3048 to 0.2032 mm (0.012 to 0.008 in.). The presence of a torn region is simulated by replacing one of the pads just described by a "slit" pad which has a 5.08 cm (2-in.) long slit at the center of each of the five DAM sheets in the pad. The "slit" pad can be placed at any one of ten depths within the stack.

The complex plane display of eddy current signals obtained from these coils and test specimens are shown in Figure 20 a, b, and c. The excitation frequency for both the 3.81 cm (1 1/2-in.) and the 7.62 cm (3-in.) diam coils is 400 kHz. The effects of changing four test variables are shown. The variables are: 1) prove lift-off, 2) separator thickness, 3) varying electrical conditions from region to region of the blanket, and 4) the presence of a slit pad at level 5 (the top or surface pad is at level 1).

ANALYSIS OF THE MULTIPARAMETER METHOD

The following analysis illustrates how the effects of three of the variables, lift-off, separator thickness (crushing), and the presence of a slit pad at level 5, can be separated. The effects of the varying conditions from point to point represented by the meandering lines in Figures 20a and 20b, are disregarded in the analysis because sufficient information can not be obtained from the loci shown.

This analysis is given as an illustration of separation rather than as a proof of separation of variables, because of uncertainties in scaling signal vector amplitudes and angles from the loci. Also, practical proof of the separation of variables must be demonstrated using instrumental means, since it is impractical to take into consideration all variations of the signals actually met in practical cases.

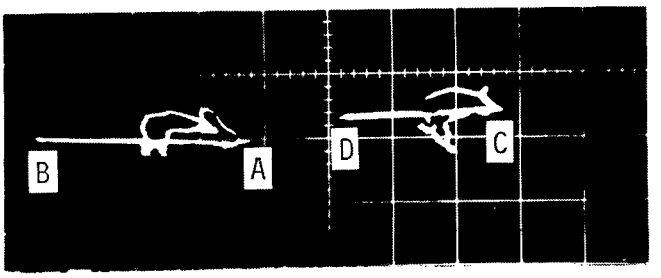

a. Coil Diameter: 3.81 cm (1 1/2 in.), Lift-Off A to B, with Separators 0.012 in. Thick; Lift-Off C to D with Separators 0.008 in. Thick; Separator Thickness Change, A to C, 0.3048 mm (0.012 in.) to 0.2032 cm (0.008 in.) Lift-Off Zero; Varying Electrical Conditions: Meandering Lines

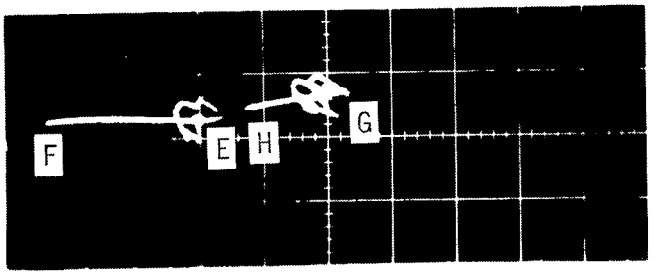

b. Coil Diameter: 7.62 cm (3 in.) Lift-Off E to F, with Separators 0.3048 cm (0.012 in.) Thick; Lift-Off G to H, with Separators 0.2032 mm (0.008 in.) Thick; Separator Thickness Change, E to F, 0.3048 to 0.2032 mm (0.012 to 0.008 in.) Lift-Off Zero; Varying Electrical Conditions: Meandering Lines

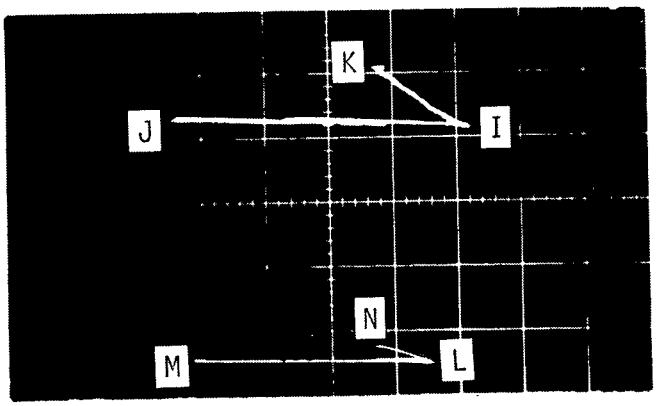

c. Upper Trace, Coil Diameter: 3.81 cm (1 1/2 in.), Lift-Off, I-J; Slit at Level 5, I-K
Lower Trace, Coil Diameter: 7.62 cm (3 in.) Lift-Off, L-M; Slit at Level 5, L-N

FIGURE 20. Complex Plane Signal Displays for 3.81 and 7.6 cm (1 1/2 and 3 in.) Diameter Inspection Coils. Excitation Frequency 400 kHz

The present analysis assumes vector point signals and the validity of the application of linear algebra. The analysis is given in considerable detail because it applies both to the single-frequency case using coils having different diameters and to the multifrequency multiparameter eddy current methods.

Complex plane display of eddy current signals obtained from these coils and test specimens are shown in Figure 21. The excitation frequency for both the 1 1/2-in. and 3-in. diameter coils is 400 kHz. The effect of changing four test variables is shown. The variables are probe lift-off, separator thickness, and the presence of a slit pad at level 5 (the top or surface pad is at pad level 1).

The vector space approach[2] is used to illustrate separation of variables. This approach, used here to illustrate the separation of variables using a single excitation frequency, is valid for the multifrequency excitation method as well. Small signal conditions are assumed, and the principles of linear algebra are applied. The changes in variables or parameters from some nominal or normal values are represented by the column matrix P]. The square matrix [A] relates the changes in the variables to the demodulated output signals of the receiver represented by the column matrix C]. The components of C] are the outputs of the amplitude-phase detectors of the receiver. The relationship between [A], P], and C] is given by the matrix equation:

$$[A]\,P] = C] \quad . \tag{1}$$

Separation or decoupling of variables or parameters P] is obtained[2] by multiplying both sides of Equation (1) by $[A]^{-1}$, by Adjoint [A], by D_a Adjoint [A] or by $D_a\,[A]^{-1}$, where D_a is any diagonal matrix having matrix elements of arbitrary nonzero. It is noted that

$$\text{Adj}\,[A] = |A|\,[A]^{-1} \tag{2}$$

where $|A|$ is the determinant of [A].

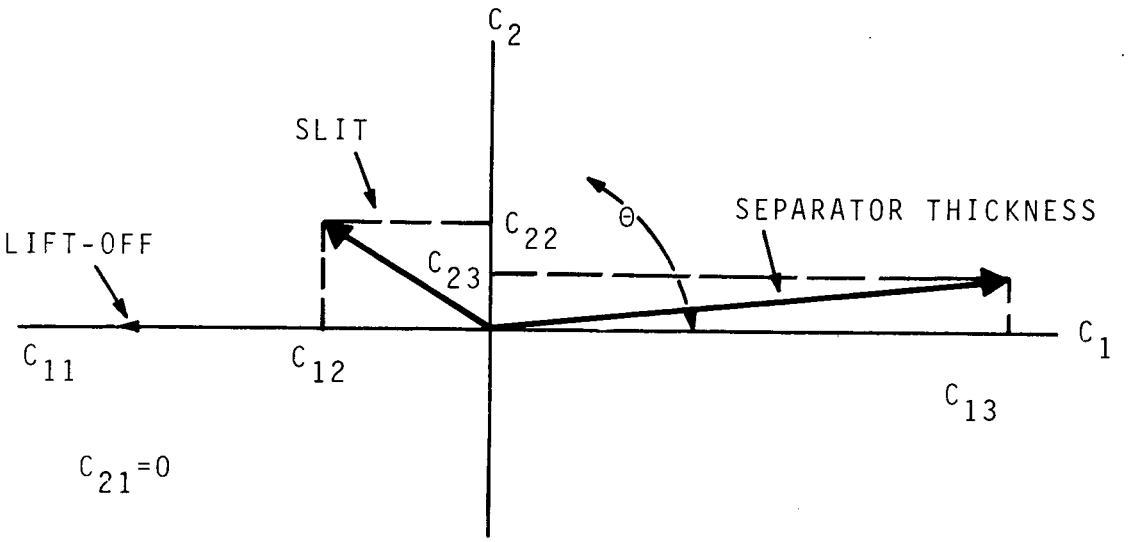

a. 3.81 cm (1 1/2 in.) Diameter Coil; Frequency 400 kHz

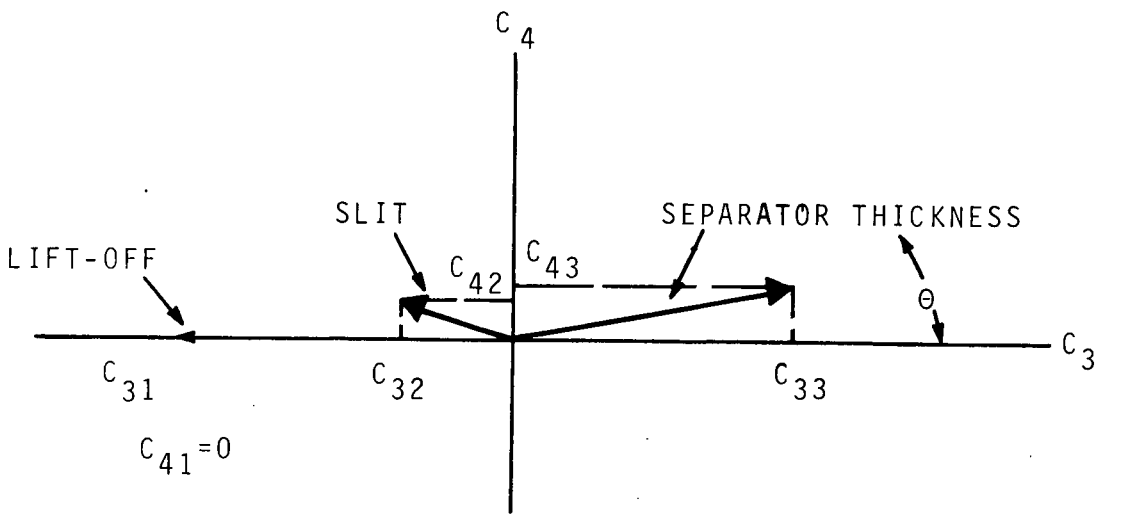

b. 7.6 in. (3 in.) Diameter Coil; Frequency 400 kHz

FIGURE 21. Receiver Output for Lift-Off, Slit at Pad Level 5, and Simulated Crushing of the 10-Pad Blanket

Multiplying both sides Equation (1) by Adjoint [A] gives

$$\text{Adj } [A]\ [A]\ P] = \text{Adj } [A]\ C] \quad . \tag{3}$$

Substitution of Equation (2) for Adj [A] gives

$$P] = \frac{\text{Adj } [A]}{|A|}\ C] \tag{4}$$

For a more complete generalization to illustrate separation or decoupling in contrast to solution of the equations, both sides of Equation (4) may be multiplied by the arbitrary diagonal matrix D_a, giving

$$[D_a]\ P] = [D_a]\ \frac{\text{Ajd } [A]}{|A|}\ C] \quad . \tag{5}$$

For the purpose of the present example, the outputs of the receiver amplitude-phase detectors are computed from the appropriate vector (or phasor) signals in Figures 20a, 20b and 20c. The vectors associated with the 3.81 cm (1 1/2-in.) diameter coils are shown in the C_1 C_2 plane in Figure 21a, and those associated with the 7.62 cm (3-in.) coil are shown in the C_3 C_4 plane in Figure 21b. The components of these vectors C_{mn}, (m = 1,... 4, n = 1,... 3) are also shown. The scale in Figures 21a and 21b is twice that of Figures 20a, 20b and 20c. A scale distance of 5.08 cm (2 in.) in Figure 21a or 21b equals 2.54 cm (1 in.) in Figures 20a, 20b or 20c. Table 1 lists the variables, the scale vector lengths A_n, vector angles θ, and source of the data.

TABLE 1. Signal Data

Variable	Vector Length, A_n	Angle θ	Source
Lift-Off	0.92	180°	Figure 21a, Left Locus
Lift-Off	0.87	180°	Figure 21b, Left Locus
Slit at Level 5	0.51	148°	Figure 21c, Upper Trace
Slit at Level 5	0.30	163°	Figure 21c, Lower Trace
Separator Thickness	1.37	6°25'	Figure 21a, (A to C)
Separator Thickness	0.75	11°43'	Figure 21b, (E to G)

The receiver outputs for a two-frequency, four-parameter system are given by the equations

$$C_{mn} = A \cos \theta \ (m = 1, 3), \ n = 1,2,3,4 \quad . \tag{6}$$

$$C_{mn} = A \sin \theta \ (m = 2, 4), \ n = 1,2,3,4 \quad . \tag{7}$$

The subscript m refers to the axis 1,2,3 or 4 in the signal 4-space or the number of the receiver output channel (phase detector output), and the subscript n refers to the parameter number. The C_{mn} for the present example are shown labeled in Figure 21.

It is noted that the receiver outputs could have been read directly at the receiver output terminals instead of computing them. The receiver outputs calculated from Equations (6) and (7) and arranged in a rectangular matrix [A], see Equation (1), are

$$[A] = \begin{bmatrix} -0.92 & -0.4287 & 1.3614 \\ 0.0 & 0.2703 & 0.1511 \\ -0.87 & -0.2869 & 0.7344 \\ 0.0 & 0.0877 & 0.1538 \end{bmatrix} \tag{8}$$

Since only three parameters are being separated in the present example, a 3 x 3 matrix is sufficient for producing the necessary decoupling or solution. A 3 x 3 matrix for this purpose is obtained by omitting the fourth row, giving:

$$[A] = \begin{bmatrix} -0.92 & -0.4287 & 1.3614 \\ 0.0 & 0.2703 & 0.1511 \\ -0.87 & -0.2869 & 0.7344 \end{bmatrix} \tag{9}$$

The determinant of this matrix is

$$|A| = 0.1540 \quad . \tag{10}$$

Thus, the matrix is nonsingular and its inverse exists. This is the necessary condition for solving the set of equations represented by Equation (1).

The Adjoint of [A] is

$$\text{Adj}[A] = \begin{bmatrix} 0.2418 & -0.0758 & -0.4328 \\ -0.1315 & 0.5088 & 0.1390 \\ 0.2352 & 0.1090 & -0.2487 \end{bmatrix} \tag{11}$$

The column matrix C] in Equation (1) represents the output signal vector. The components of this vector are the amplitude-phase detector outputs of the receiver. The components of the column vector C] may be written as sums of the individual phase detector outputs for the three parameters as follows:

$$C] = \begin{matrix} C_{11} + C_{12} + C_{13} \\ C_{21} + C_{22} + C_{23} \\ C_{31} + C_{32} + C_{33} \end{matrix} \quad . \tag{12}$$

Subscripts are the same as in Equations (6) and (7) and in Figure 2.

The separation or decoupling of variables, predicted by the existence of the determinant of [A] Equation (10), can now be shown by multiplying Equation (12) by Equation (11), substituting in Equation (12) the numerical values of the C_{mn}.

$$\begin{bmatrix} 0.2418 & -0.0758 & -0.4328 \\ -0.1315 & 0.5088 & 0.1390 \\ 0.2352 & 0.1090 & -0.2487 \end{bmatrix} \begin{bmatrix} (-0.92 & -0.4247 & +1.3614) \\ (\ 0.00 & +0.2703 & +0.1511) \\ (-0.87 & -0.2869 & +0.1538) \end{bmatrix} =$$

$$\begin{bmatrix} (0.1540 & +0.0000 & +0.0001) \\ (0.0000 & +0.1540 & +0.0001) \\ (0.0000 & +0.0000 & +0.1540) \end{bmatrix} \quad . \tag{13}$$

The right hand part of Equation (13) shows the separation of variables. Parameter 1 is indicated only in row 1, Parameter 2 only in row 2, and Parameter 3 only in row 3. These three rows correspond to the three output channels of the transformation circuit of the multiparameter eddy current instrument.

PRACTICAL PROBLEMS ON FULL SCALE TANKS

The evaluation of high performance insulation (HPI) on full scale tanks presents many practical problems. The experimental work described in this report was performed under laboratory conditions, and additional test variables can be present during the evaluation of insulation on full scale tanks. Some additional variables which may be present are:

- Variation in spacing between insulation blankets and tank
- Variation in spacing between blankets
- Presence of metallic supports and tubing
- Varying contour or curvature of tank
- Varying thickness of tank
- Presence of magnetic materials
- Presence of purge bag which may limit access
- Proximity of vehicle structure, and variations in spacing between it and the tank and insulation
- Variation in positions of blankets which do not adversely affect serviceability but which may affect instrument readings
- Development of scanning technique which assumes accuracy of periodic measurements and calibration; sensing coils, if mounted permanently must withstand 300°F temperature.

The inspection problems are most severe if it is necessary to inspect the insulation with the tank in place within the vehicle. In this case, major constraints exist on a scanning technique because of limitation of space. The presence of the purge bag may interfere with scanning the insulation with a probe whether or not the tank can be removed. If impelling reasons exist for not removing the tank together with its insulation; sensing coils could be installed at selected positions and connected to inspection cable connectors. The simplest system of this type would have inspection coils mounted on or in the surface of the outer blanket. The coils would then be switched sequentially to the instrument system.

MECHANICAL FIXTURES FOR SCANNING LARGE TANKS

Scanning requirements differ greatly depending on whether or not the tank can be removed from the vehicle. The simplest arrangement prevails if the tank can be removed and mounted on a rotating mechanism as shown in Figure 22. The tank would be rotated and sensing probes automatically adjusted to programmed positions. Instrument readings would be recorded before the first flight and each subsequent flight. Multiple inspection coils and associated positioning mechanisms could be provided to decrease inspection time.

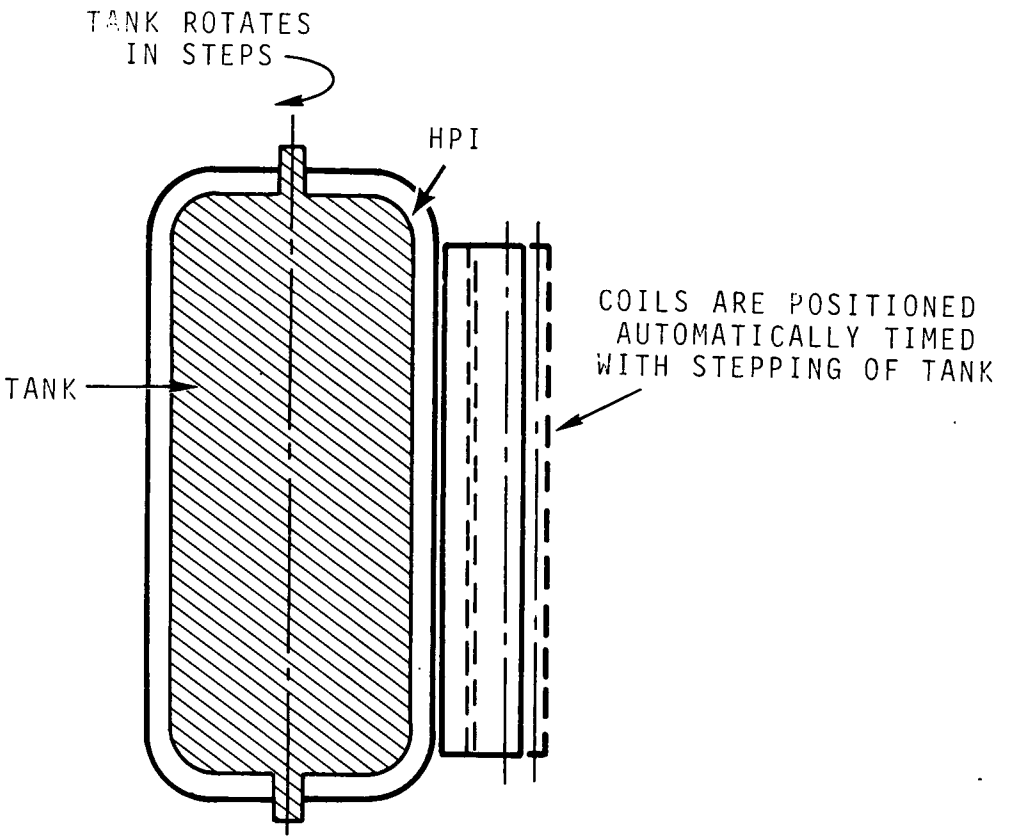

FIGURE 22. Inspection of HPI (Tank Removed from Vehicle)

If the tank cannot be removed from the vehicle, the scanning problem is more involved as exemplified by Figure 23. The inspection coils and their positioning arms must of necessity avoid any obstruction as they are moved along their required trajectory. A critical variable here is the maneuvering room available for the coils and positioning arms. The available entry areas and their relationships to the areas to be scanned are especially important. Mechanical problems in regard to positioning arm linkage may make this approach not feasible. At least some regions may not be accessible. Figure 24 depicts the more practical arrangement using permanently mounted coils attached to the face of the outer blanket.

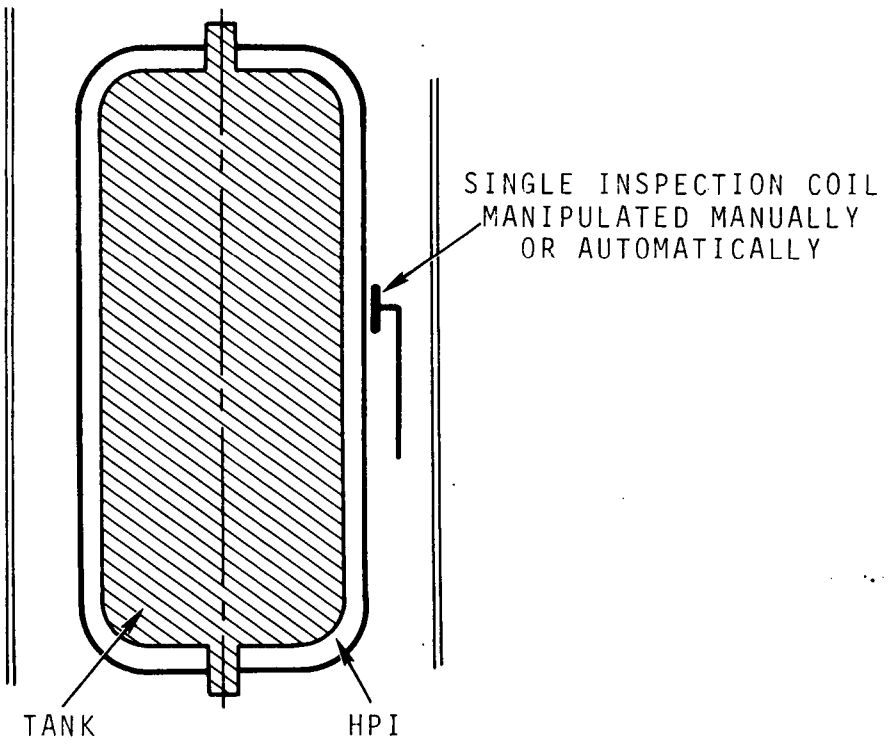

FIGURE 23. Inspection of HPI (Tank Within Vehicle)

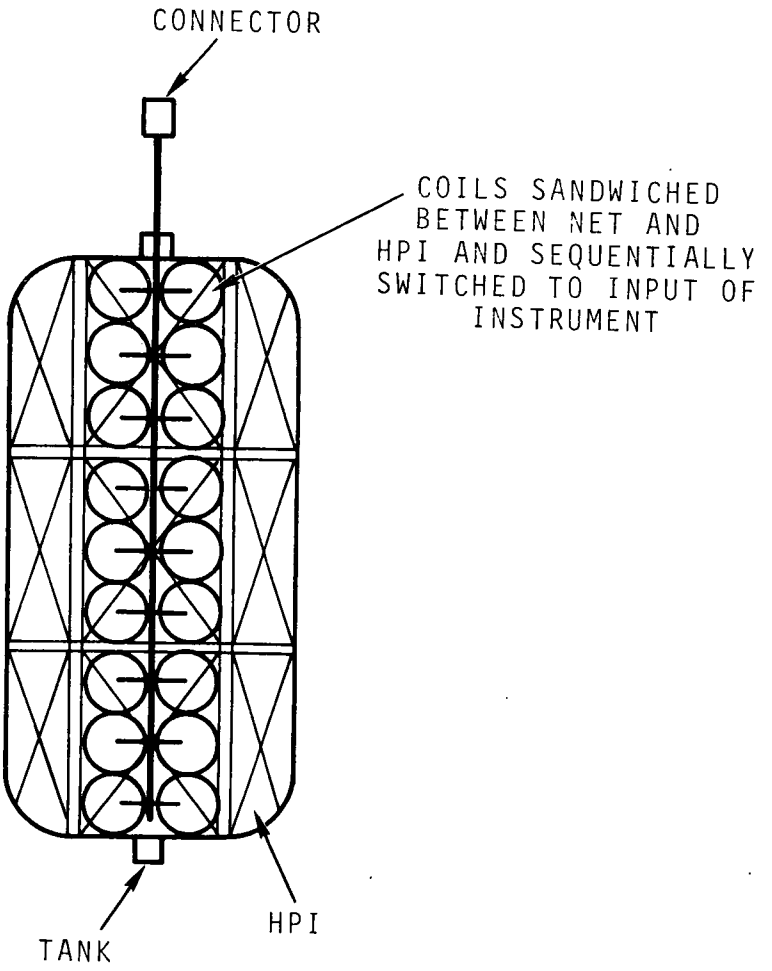

FIGURE 24. Inspection of HPI with Coils Permanently Mounted on or in the Outer Surface of the Outer Blanket

CHARACTERISTICS ESSENTIAL FOR PROTOTYPE INSTRUMENTATION SYSTEM

The experimental results of the present program indicate that the prototype system should be an electromagnetic multifrequency inspection system whose operation is based on eddy current multiparameter nondestructive test principles.

Important characteristics of the prototype system are listed below.

- It should distinguish between compression of blankets and the presence of tears and corroded areas.

- Its effectiveness should not be reduced by variation in spacing between blankets and tank, and variation in reflector characteristics.
- Simplicity of calibration and operation adjustments should be emphasized.
- Reproducibility of readings should be maintained from flight to flight. Inspection coils, mountings and fixtures should withstand severe environmental changes.
- Information storage capacity is needed to retain inspection results for comparison purposes.

The results of the present program show that the manual adjustment of the calibration controls for the four-parameter system requires a prohibitive amount of time. A high degree of operator skill is also needed. Increasing the number of variables will place additional burden on the operator, making it necessary to provide for automatic calibration of the equipment. Two main approaches for accomplishing them are by replacing the present manual calibration system with an off-line computer or an on-line computer. A block diagram of a system using a large off-line digital computer is shown in Figure 25. An on-line computer system is shown in Figure 26.

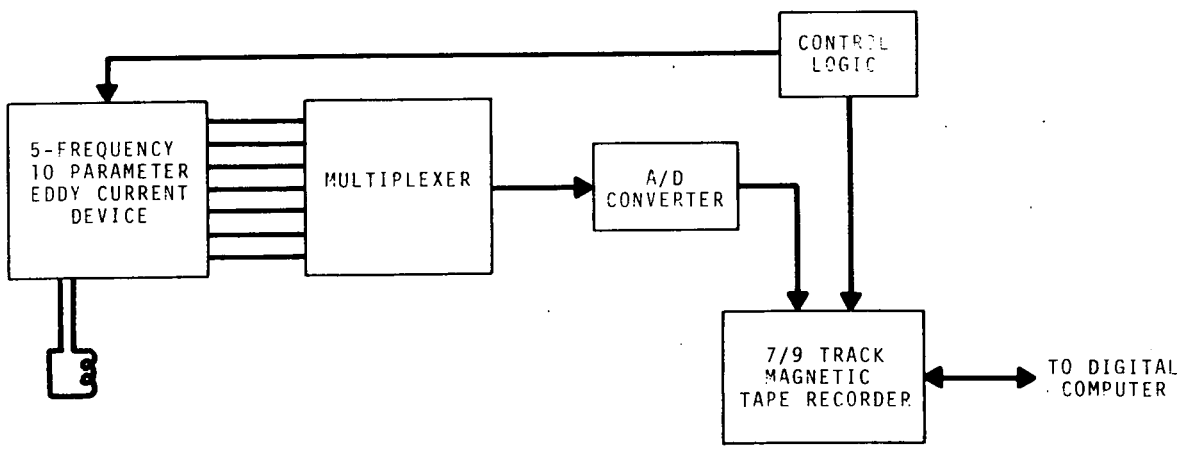

FIGURE 25. Off-Line Digital Computer System

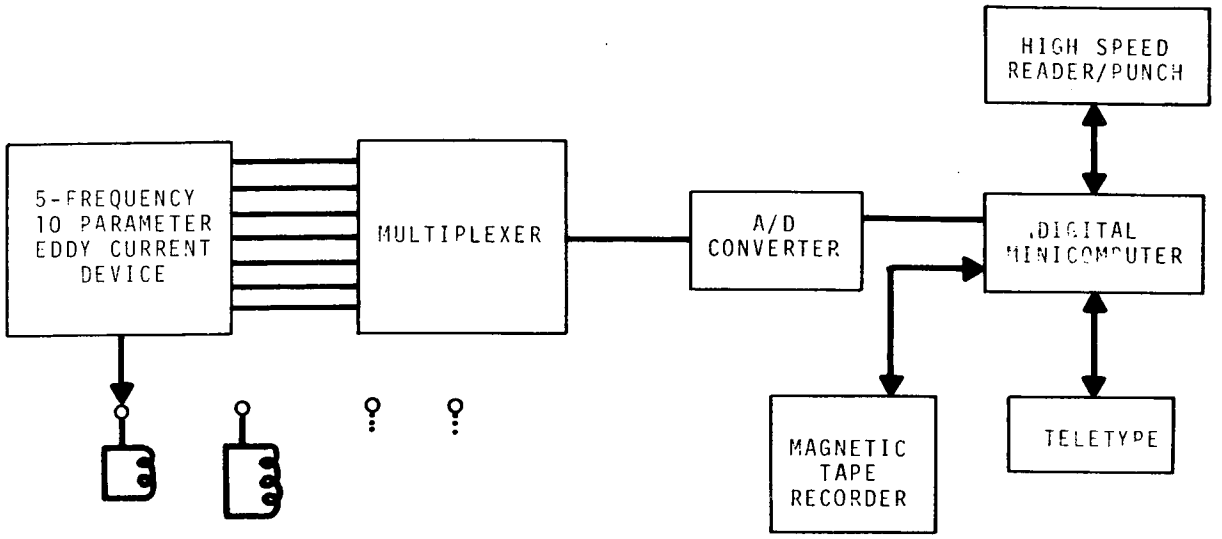

FIGURE 26. On-Line Digital Computer System

PHASE II. APPLICATION TO ADDITIONAL MATERIALS

The material supplied by NASA for use in evaluating the selected technique is double-goldized kapton (DGK), already mentioned in connection with Figures 7 and 8d, and referred to by the designation DGK-1. This composite varies more in electrical characteristics, and possibly in thickness or in conductivity, than the other composites inspected. Figure 7 shows that the DGK-1 material appears to be either thicker or having a higher thickness-conductivity product than the DAM-2 or DAM-3 composite material. Thus, lower operating frequencies will be required for the goldized material than for the DAM-2 and DAM-3 material assuming all have the same number of layers per blanket. It is also noted that the DAM-1 material supplied by NASA is approximately comparable to the DGK-1 material. Eddy current measurements made using a stack of 50 sheets of DAM-2 composite showed that a 10% slit (5 slitted sheets in a stack of 50 sheets) could be detected with the two-frequency system operating at 100 kHz and 300 kHz. A much lower frequency is required to obtain comparable results using 50 sheets of the DGK-1 or DAM-1 material because of their higher thickness-conductivity products. Frequencies of 5 kHz and 15 kHz would be reasonable as the depth of eddy current penetration varies approximately as the inverse square of frequency.

Measurements with 10 sheets of the DGK-1 material at a single frequency of 100 kHz using a 5.08 cm (20 in.) diameter inspection coil show that one sheet with a 5.08 cm (20 in.) long slit at its center could be detected. Figure 27 shows that the slit region produces signals significantly different than those produced by the regions not near the slitted region. These regions not near the slit are at the corners of a square, having sides 10 cm (4.0 in.) long, centered around the slit region. The effect of replacing the slitted sheet with a sheet of DGK-1 without a slit is shown in Figure 28. It was expected that the new signal could appear within the four spot group representing the more normal regions, that is, regions not near

the slit location. However, the new signal appeared between the four spot group and the group of three readings obtained from the slit. This indicates a significant variation in signals caused by differences in DGK-1 sheets.

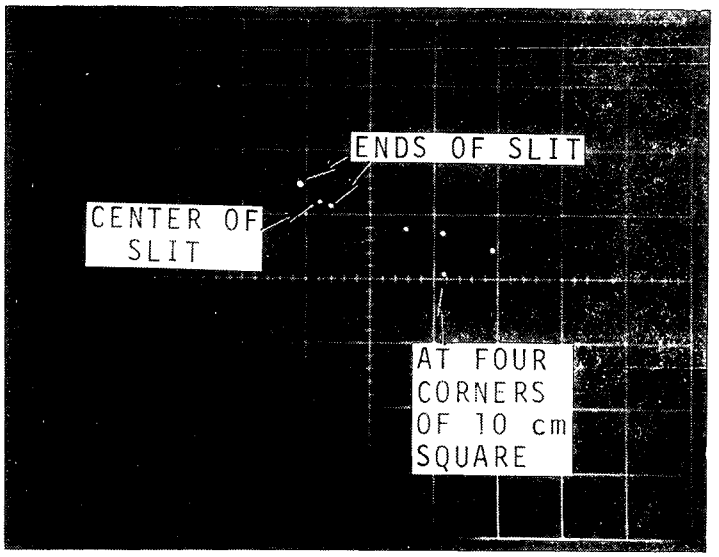

FIGURE 27. Detection of Slit in Sheet No. 5 in a Stack of 10 Sheets of DGK-1

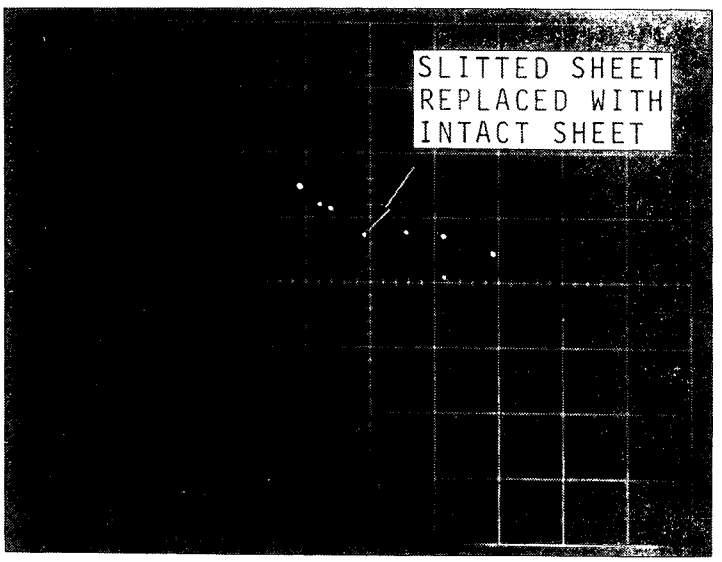

FIGURE 28. Sheet No. 5 Without Slit in a Stack of 10 Sheets of DGK-1

The foregoing measurements made with a stack of only 10 sheets of the DGK-1 material using a single operating frequency do not confirm the ability of the multifrequency eddy current system to discriminate between several variables of a simulated blanket made of DGK-1 as has been shown for the DAM-2 material in Figures 11 to 19. A second set of measurements using the multiparameter principle were made to demonstrate discriminating ability. The test specimen was made of a stack of 50 sheets of the DGK-1 material, using 0.1016 mm (0.004 in.) thick paper separators. Lower operating frequencies were chosen than for use with the DAM-2 composite because of the higher thickness-conductivity product of the DGK-1 material. The operating frequencies are 15.6 kHz and 31.2 kHz, and the inspection coil is a 5.08 cm (2.0 in.) in diameter. The instrument was calibrated to discriminate against inspection coil lift-off signals, a small amount of blanket compression, and signal variations caused by variations in DGK-1 material around a 10 cm (4 in.) square region around the slitted region. Fine slitted sheets are used, with 5.08 cm (2.0 in.) long slits, replacing fine sheets without slits midway down the stack of 50 sheets.

The results are shown in Figure 29. Signals from variations in the DGK-1 material were quite large and were difficult to discriminate against, and still show some residue in the material direction. The pattern is oriented so that the signals being discriminated against produce deflections mainly in the horizontal direction.

Figure 30 shows the results obtained under the same instrument adjustments for Figure 29, but with the inspection coil on the opposite side of the blanket. Good discrimination is still obtained. The blanket and inspection coil were then returned to original position, and all reflector sheets above those containing the slits were rotated 180 degrees. The discrimination against the variation in the DGK-1 sheets was now found to be degraded as is shown in Figure 31. This highlights the complexity of the problem of variations within each reflector sheet and the resulting variations as a function of depth within the blanket.

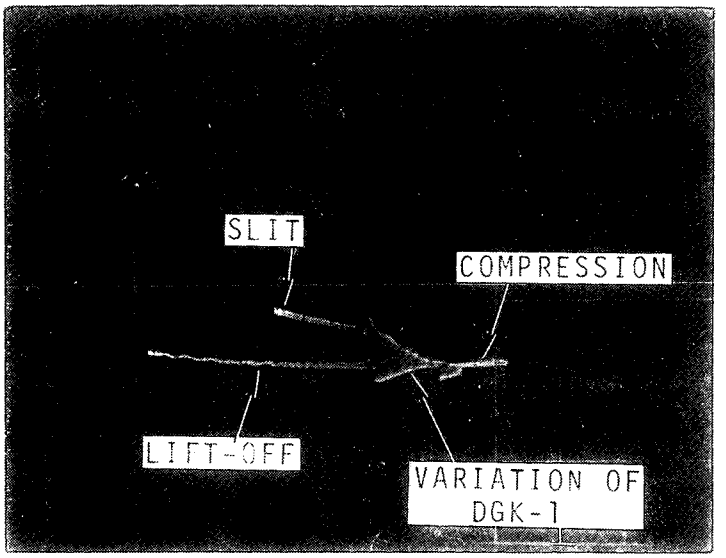

FIGURE 29. Detection of Slits in 5 Sheets Midway Down a Stack of 50 Sheets of DGK-1. Discrimination against inspection coil lift-off, blanket compression, and variation of properties of DGK-1. Frequencies 15.6 kHz and 31.2 kHz.

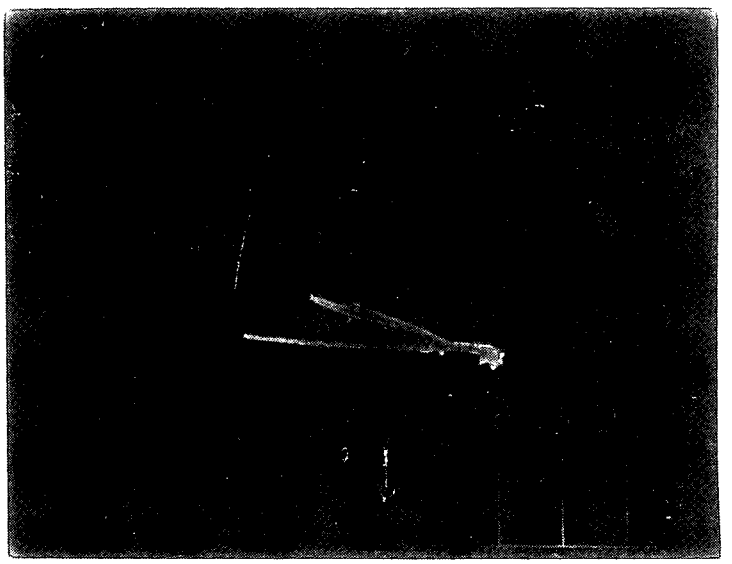

FIGURE 30. Instrument Conditions Same as in Figure 29, but with Inspection Coil on Opposite Side of Simulated Blanket

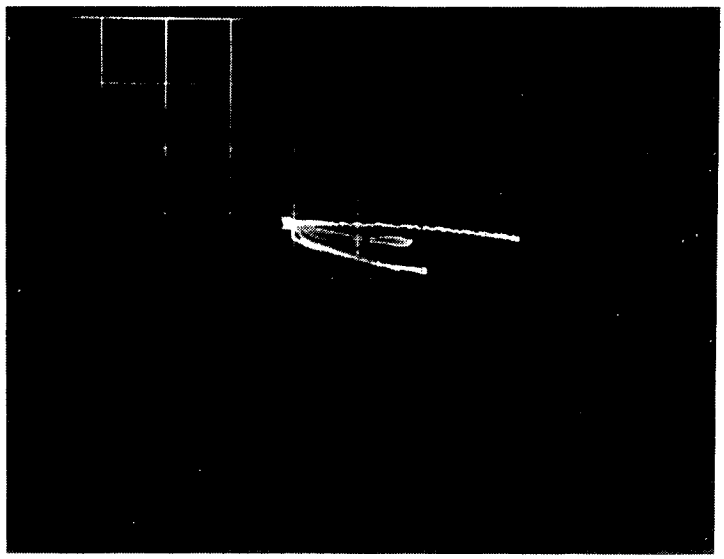

FIGURE 31. Instrument Conditions Same as in Figure 29, but with Upper 22 Sheets Rotated 180 Degrees

EFFECT OF TANK WALL

It was found that placing a 0.635 cm (0.25 in.) thick sheet of austenitic stainless steel beneath the stack of 50 sheets of DGK-1 material interfered with the discrimination shown in Figure 29. This indicates that the presence of the tank wall and the variation of spacing between it and the blanket constitute an additional variable. At least one additional operating frequency will be needed to reduce this undesired effect.

EFFECT OF WATER

From a theoretical viewpoint there should be no direct effect on the inspection of HPI using the electromagnetic method. The ac impedance of water at the frequencies used is very large compared with that of the metallized coatings in the HPI, thus very little effect is possible. However, an indirect effect is possible if the water causes a swelling or shrinkage of the separator material or actually forces the reflector layers apart as a result of its presence.

These factors were checked experimentally using a stack of ten DAM-1 reflector sheets separated by one layer of face netting. The fifth sheet contained a slit 5.08 cm (2.0 in.) in length. A 5.08 cm (2.0 in.) diameter inspection coil was used, operating at 100 kHz and 300 kHz. The multi-parameter method is used and the instrument adjusted to discriminate against inspection coil lift-off and some variations of reflector material. Test results of this dry arrangement are shown in Figure 32, in which the slit signal is the one having the largest vertical deflection. The whole blanket assembly was then reassembled under water, and the water permeated between each reflector sheet. The top sheet and coil were under about 2.54 cm (1.0 in.) of water.

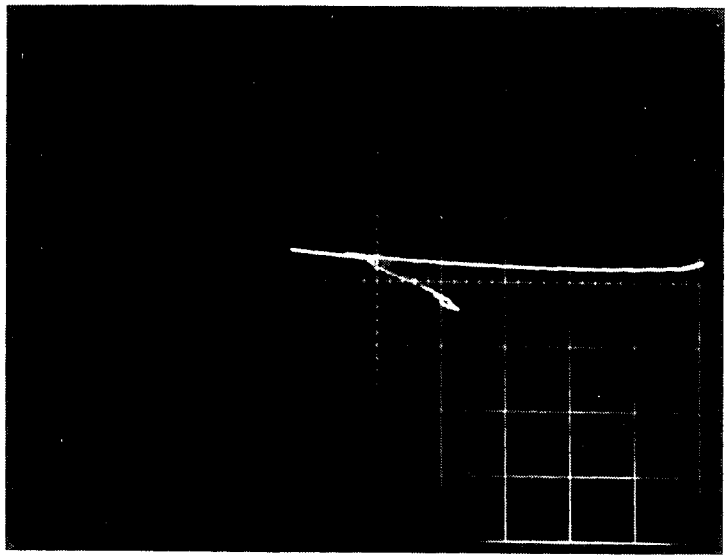

FIGURE 32. Detection of Slit in Reflector, Dry Simulated Blanket

The slit was still detected without readjustment of the instrument controls. The signals obtained for the immersed conditions are shown in Figure 33. Some perturbations of the signals were observed which were caused by the tendency of the top layers of the reflector to be separated by the presence of water between them.

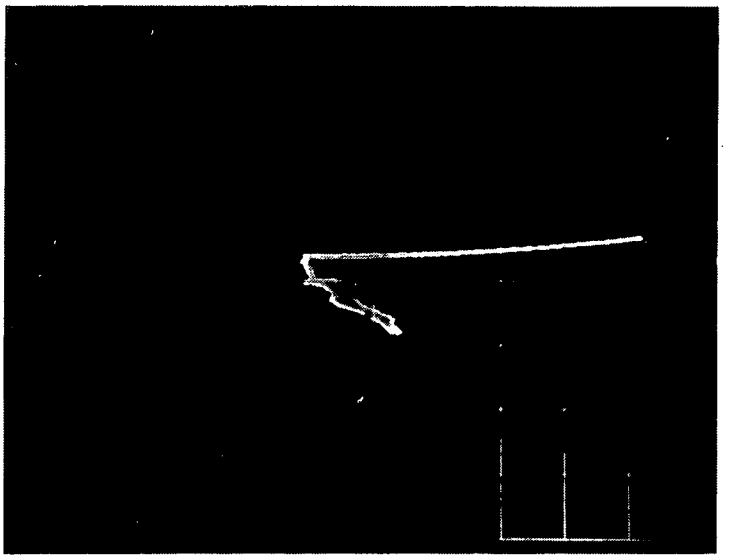

FIGURE 33. Detection of Slit in Reflector, Simulated Blanket and Inspection Coil Immersed in Water

ACOUSTICAL MEASUREMENTS

Another technique investigated for evaluation of multilayer insulation was the use of low frequency acoustic techniques. These techniques had previously been used to determine the presence of good bonding between foam insulation in the tank wall and for determining voids in the foam. It was suggested that this technique might be modified to inspect multilayer insulation. Two complicating factors in this case, the layered form of the insulation including the face net, and the fact that bonding between the tank wall and the insulation is not required, make the tests considerably more difficult.

A system was set up for measurements of the acoustic responses function of frequency of a simulated tank insulation problem (see Figure 34). A constant amplitude signal generator and wideband power amplifier were used to drive a speaker. The through transmission response to the system was measured with a microphone and an audio spectrum analyzer for the cases of no aluminum sheet, with aluminum sheet, and with aluminum sheet and DAM insulation sheets. These preliminary results showed that considerably more

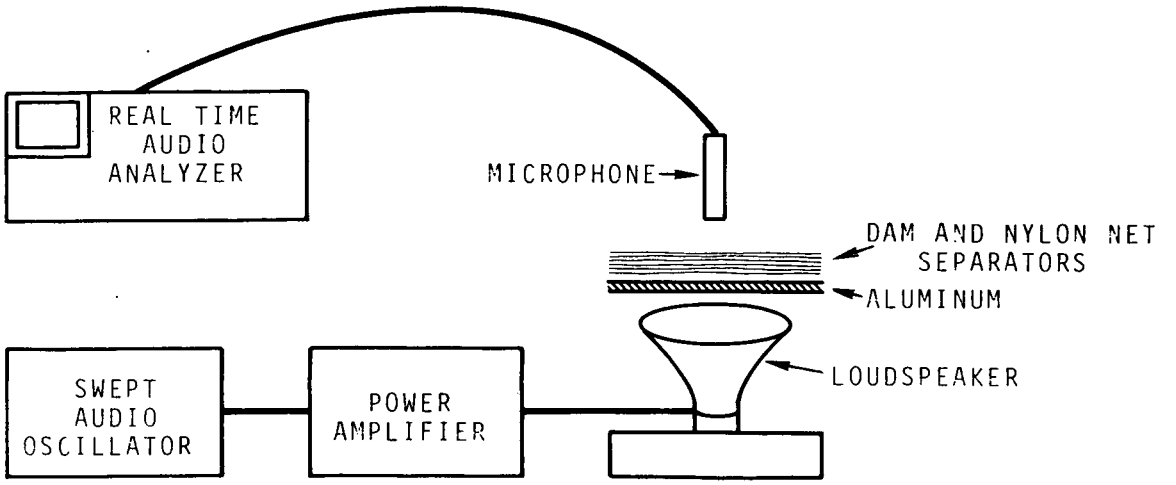

FIGURE 34. Block Diagram of Acoustic Test System

development of the system would be necessary for definitive results. Because of lack of time and funding and because of a desire to place the emphasis on the eddy current portion of this test where more success was realized, these developments were not undertaken. The problems of the loose, uncoupled, aluminized or metallized sheets appear to make the test difficult to instrument. Further acoustic tests were therefore discontinued.

THERMAL MEASUREMENTS

Thermal measurements were made by placing good and torn/corroded layers of double-aluminized mylar (DAM) in sequence over a heated tank and then scanning the emitted radiation from the front sheet.

EXPERIMENTAL RESULTS

An experiment to determine the sensitivity of the infrared technique to worn and corroded samples of double-aluminized mylar (DAM) was set up as shown in Figure 35. The tank had flat glass sides and dimensions of roughly 30 x 30 x 20 cm (12 x 12 x 8 in.). Round samples (~30 cm--12 in. diam) of DAM were placed on the 30 x 30 cm (12 x 12 in.) face of the tank. Nylon net separators were used to reduce direct conduction between

DAM layers. Water at a temperature of 55°C was placed in the tank; ambient temperatures were about 20°C. A high-speed infrared scanner (AGA model 680) was used to image the emitted radiation from the test setup. The scanner has a spatial resolution of 1.3 milliradians and a temperature resolution of 0.2°C. It scans at 16 frames per second; one half second exposures were used on the accompanying photographs.

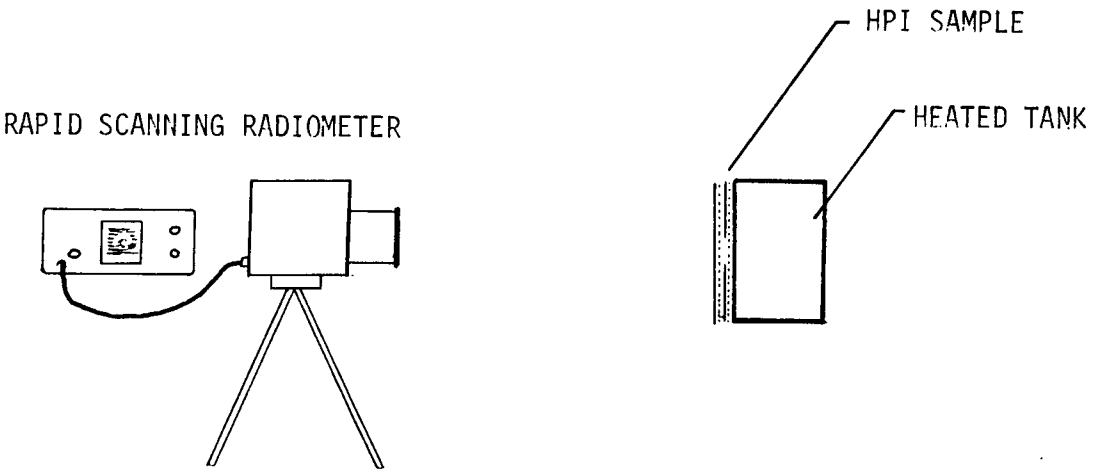

FIGURE 35. Thermal Testing of HPI Insulation for Corrosion and Tearing

Figure 36 shows infrared scans of a DAM sheet in a darkened room. The high reflectivity of the sheet (99.95%) reflects any temperature differences of the surrounding area. For example, the apparent increase in temperature in the right-hand photograph of Figure 36 is not a real increase but is merely the reflection of the operator's hand moved near the DAM sheet. Reflections such as these would mask any temperature differences due to anomalies in the insulation.

To reduce these reflections, the outer layer can be sprayed with a paint that has low reflectivity in the spectral region of interest, or since spraying may be undesirable on the insulation, a painted layer can be temporarily placed over the insulation.

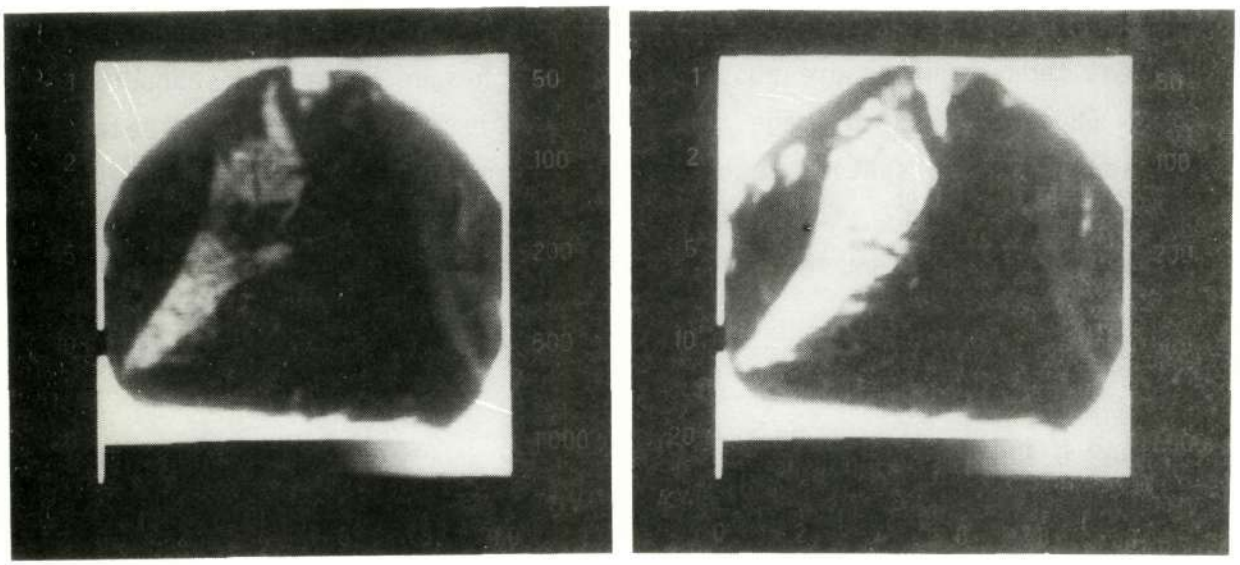

FIGURE 36. Infrared Scans of Circular DAM Sample Illustrating Reflection of Surrounding Radiation. Temperature span 10°C, center temperature 25°C.

To determine the sensitivity limits of this method the following experiment was conducted. A diamond-shaped hole approximately 10 x 10 cm was cut in one sheet of DAM. This was placed over the heated tank and an infrared scan of this is shown in Figure 37. The temperatures can be determined from the gray scale across the bottom of the photograph. The temperature span is indicated on the side of the photograph by noting the break in the border. In this temperature range the bottom scale is linearly related to the temperature, that is, for a 10-degree span each 0.1 unit on the scale represents 1.0 degree. The center temperature is determined by using a known temperature source.

The center temperature was lowered for the scan in the upper right-hand corner of Figure 37 and two tears emanating from corners of the diamond can be seen.

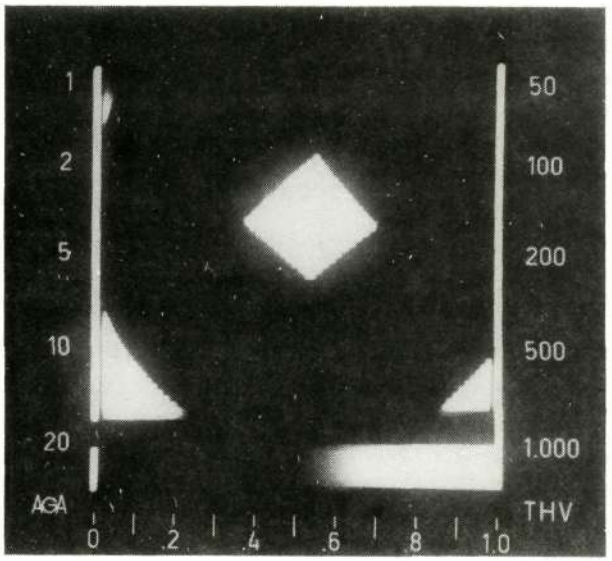

T. span 20°C, T. center 50°C

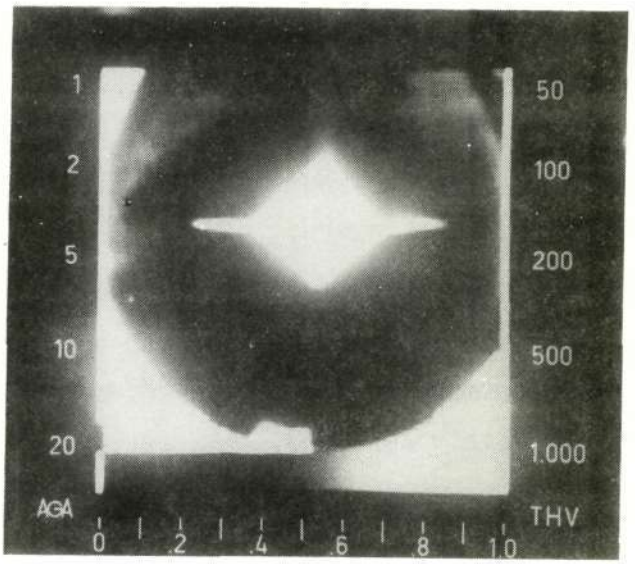

T. span 20°C, T. center 20°C

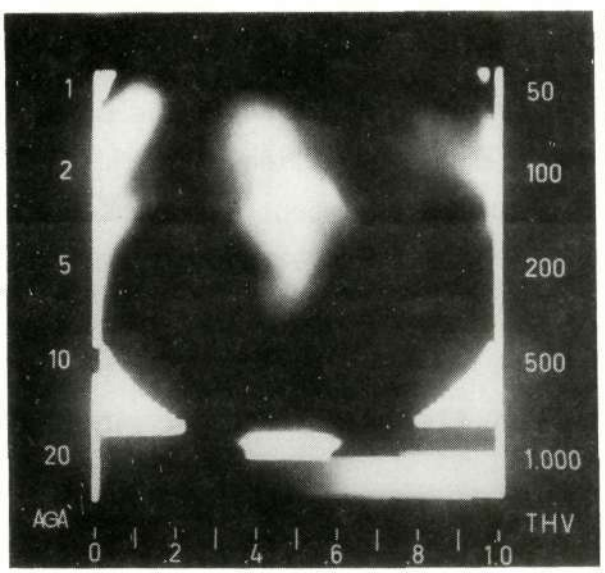

T. span 10°C, T. center 30°C

One cover layer

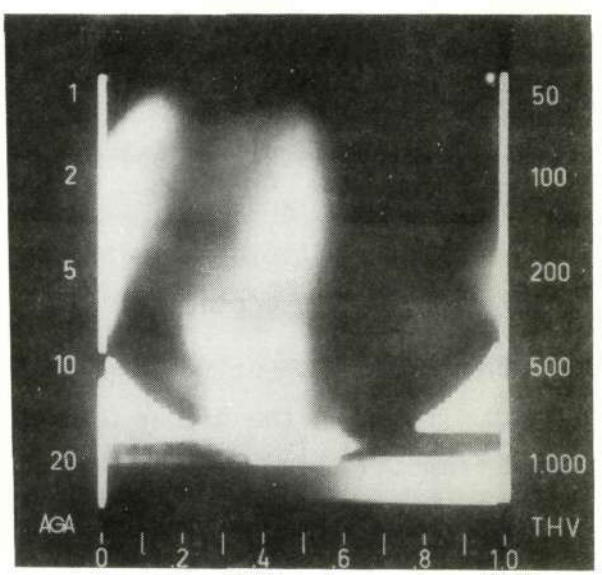

T. span 10°C, T. center 30°C

Two cover layers

FIGURE 37. Infrared Scans of Circular DAM Sample Illustrating Effect of Severe Corrosion and Subsequent Covering by Intact Layers

The hole was still visible when one layer (with a painted front surface) was placed over it. Nylon net separators separated each layer and the first layer from the tank. When two layers were placed over the hole it was obscured by other indications. These other indications are due to reflections from the room or conduction of heat through the separators and gas between the layers.

These results indicate that this through-transmission steady-state approach is not applicable to testing of multi-layer insulation as long as two or more undegraded layers cover the rest, even if the inner layers are completely corroded.

THERMAL MODEL MATHEMATICAL ANALYSIS

A simplified model of multi-layer insulation was analyzed mathematically to determine the difference in emitted radiation between intact sections and torn or corroded sections of the insulation. The analysis was made as follows. The heated tank (with emissivity of one) emits F_o watts/cm^2. The first layer of DAM (the separator is ignored) reflects most of the radiation and transmits F_1. If we let the transmissivity equal the emissivity (that is, assume no absorption or internal reflections) then $F_1 = \varepsilon^2 F_o$ plus a larger term since εF_o is trapped between the layers and must escape by multiple reflections. If $\varepsilon << 1$ the sum of the reflections passing out of the second layer is $F_2 = \varepsilon F_o/2$.

When a third sheet is added multiple reflections must be taken into account. Ignoring the higher order terms, we find that the energy transmitted from the third layer is

$$F_3 = \sum_{n=1}^{\infty} \frac{\varepsilon F_o}{4^n} = \frac{\varepsilon F_o}{3} \quad . \tag{1}$$

Analysis becomes more complicated as the number of layers increases, but it can be shown that the radiation emitted from the nth layer is

$$F_n \leq \frac{\varepsilon F_o}{n} \quad . \tag{2}$$

Many assumptions have been made in determining this figure, but they are all believed to be made on the conservative side.

If all other parameters could be neglected a radiometer could tell if a layer were missing no matter what the total number of layers. However, effects such as detector noise, background emission, etc. must be considered. The most important of these is the reflection of background emission. Temperature differences in the room which are reflected from the front layer of insulation (which has been sprayed black to reduce these reflections) produce differences in emitted radiation of $\Delta F_r = r\,\sigma\,(T^4 - T_o^4)$ where r is the reflectivity of the front layer ($r = 1-\varepsilon$) and σ is the Stefan-Boltzmann constant.

We can now compare these reflections to differences in radiation caused by missing or corroded layers. At room temperature, $\Delta F_r \sim 6 \times 10^{-4} r$ watts/cm^2/°K. The reflectivity of the front insulation layer is about 0.05 so that $\Delta F_r = 3 \times 10^{-5}$. The tank, heated to 55°C, emits 6×10^{-2} watts/cm^2. If $\varepsilon = 0.03$ then 1.8×10^{-3} watts/cm^2 will be transmitted through one layer. As the number of layers increases, however, the change in emitted radiation caused by each layer becomes progressively smaller. The difference between six and seven layers is approximately 3×10^{-5} watt/cm^2 which is the same as differences caused by only a one degree variation in the area surrounding the test.

These rough calculations reinforce the experimental results and indicate that this particular thermal setup is not applicable to the testing of multi-layer insulation blankets composed of many layers of low emissivity materials.

REFERENCES

1. D. R. Krause, Development of Lightweight Material Composites to Insulate Cryogenic Tanks for 30-Day Storage in Outer Space. First Quarterly Report, June 1, to September 1, 1970, MDC G0683, McDonnell Douglas Astronautics Company-West, Huntington Beach, California.

2. H. L. Libby, Broadband Electromagnetic Testing Methods, Part IV, Multiparameter Test Principles, BNWL-953, Pacific Northwest Laboratories, Richland, Washington, January 1, 1969.

3. H. L. Libby, Introduction to Electromagnetic Nondestructive Test Methods, Wiley-Interscience, New York, 1971.

4. H. L. Libby and C. W. Wandling, Multichannel Eddy Current Tubing Tester, BNWL-765, Pacific Northwest Laboratories, Richland, Washington, May 28, 1968.

5. V. G. Vyakhorev, V. G. Gerasimov, V. P. Deniskin, L. I. Trakhtenberg and Y. M. Shkarlet, "Some Possibilities of the Eddy Current Method of Multi-Parameter Testing of Structural Components," (in Russian) in Nondestructive Testing in Nuclear Energy, Vol. 1, IAEA Vienna, pp. 115-136, 1965. For English translation see: Sci. Tech. Aerospace Report N66-34162, 1966.